Computational Design of Creep-Resistant Alloys and Experimental Validation in Ferritic Superalloys

Investigators: Peter K. Liaw[1], Mark D. Asta[2], Gautam Ghosh[3], David C. Dunand[3], Morris E. Fine[3], and Chain T. Liu[4]

Ph.D. Students: Shenyan Huang[1], Zhenke Teng[1], Zhiqian Sun[1], and Michael Rawings[3]

Research Associate: Gongyao Wang[1]

1. Department of Materials Science and Engineering, The University of Tennessee (UT), Knoxville, TN 37996, USA
2. Department of Materials Science and Engineering, University of California (UC), Berkeley, CA 94720, USA
3. Department of Materials Science and Engineering, Northwestern University (NU), Evanston, IL 60208-3108, USA
4. Department of Materials Engineering, Auburn University, Auburn, AL 36849, USA

Acknowledgement

We are very grateful to:

(1)Richard Dunst,
(2)Veto Cedro, and
(3) Patricia Rawls for their kind support.

(4) National Energy Technology Laboratory (NETL) for sponsoring this project.

Outline

- Technical Background of the Project
- Potential Significance of the Results of the Work
- Statement of Project Objectives
- The Project Team
- Previous Results
- Technical Approach to Achieve the Project Goals
- Project Budget and Schedule
- Project Management Plan
- Project Risks and Risk Management Plan
- Conclusions

Technical Background of the Project

Ferritic Alloys as Candidates for Steam Turbine (1)

Why ferritic steels? Why not Ni-based alloys?

- 80% of all electricity generation in the world is by use of steam turbines. Low cost materials are required.

- The materials with good thermal conductivity and low thermal expansion are preferable for thick section components of the steam turbine.

	Thermal Expansion Coefficient [2]	Thermal Conductivity[3]	Cost ($/t) [4]
Ferritic steel	**$1.0 \times 10^{-5}\ K^{-1}$**	**50 W/(m·K)**	**< $900**
Ni-based superalloy	**$1.8 \times 10^{-5}\ K^{-1}$**	**21 W/(m·K)**	**> $40K**

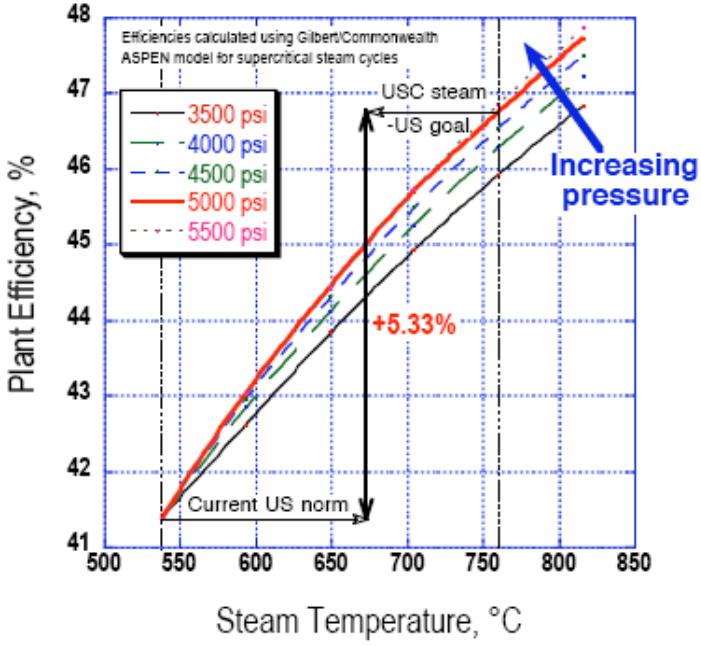

P. Maziasz, I. Wright, J. Shingledecker, T. Gibbons, R. Romanosky, *Proceedings from the fourth international conference on advances for materials technology for fossil power plants* 2005.

[1] http://en.wikipedia.org/wiki/Steam_turbine
[2] http://www.handyharmancanada.com/TheBrazingBook/comparis.htm
[3] http://en.wikipedia.org/wiki/List_of_thermal_conductivities
[4] http://www.ttiinc.com/page/ME_Materials

Ferritic Alloys as Candidates for Steam Turbine (2)

Why not conventional carbide-strengthened ferritic steels?

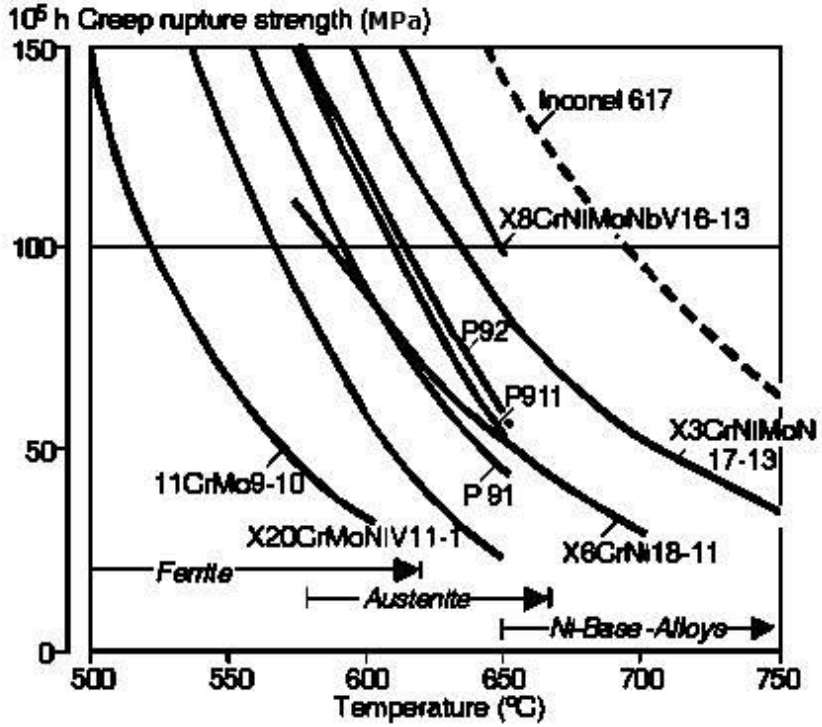

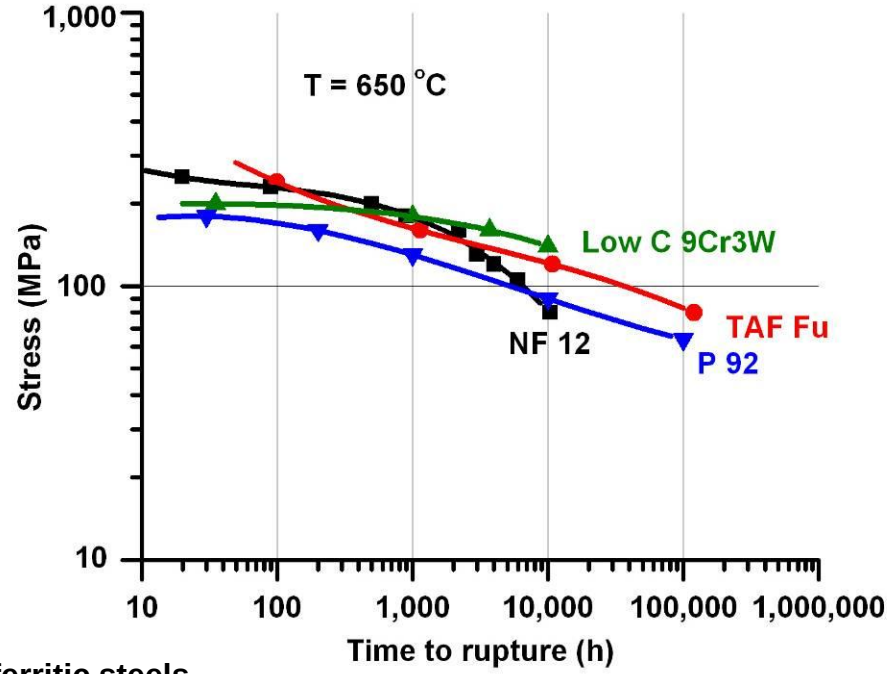

Compositions of the recently developed creep-resistant ferritic steels

Alloy	C	Si	Mn	Al	Cr	Ni	Mo	W	V	Nb	B	N
T/P91	0.08	0.2	0.3	0.04	8	0.4	0.85	-	0.18	0.06	-	0.03
T/P911	0.09	0.1	0.3	0.04	8.5	0.1	0.9	0.9	0.18	0.06	0.005	0.05
T/P92	0.07	0.5	0.3	0.04	8.5	0.4	0.3	1.5	0.15	0.04	0.001	0.03
NF12	0.09	0.03	0.5	-	12	0.5	0.13	2.6	0.2	-	0.002	0.05
TAF	0.18	0.3	0.5	-	10.5	-	1.5	-	0.2	0.15	0.03	-

P92 (9Cr0.6Mo2W) has moved the application of ferritic steels into the range of austenitic steels. However, in long-term creep tests, those materials exhibited sigmoidal-creep behavior due to the strengthening carbides coarsening or dissolving. So far no ferritic alloys demonstrated superior long-term creep resistance than P92.

Ferritic Alloys as Candidates for Steam Turbine (3)

Why B2 or/and $L2_1$ precipitates strengthened ferritic steels?

Phase	Structure	Lattice Parameter (nm)
α-Fe	Body-Centered-Cubic (BCC)	0.28665
NiAl	B2 (ordered BCC)	0.28864
FeAl	B2 (ordered BCC)	0.289
Ni_2TiAl	$L2_1$	0.5865

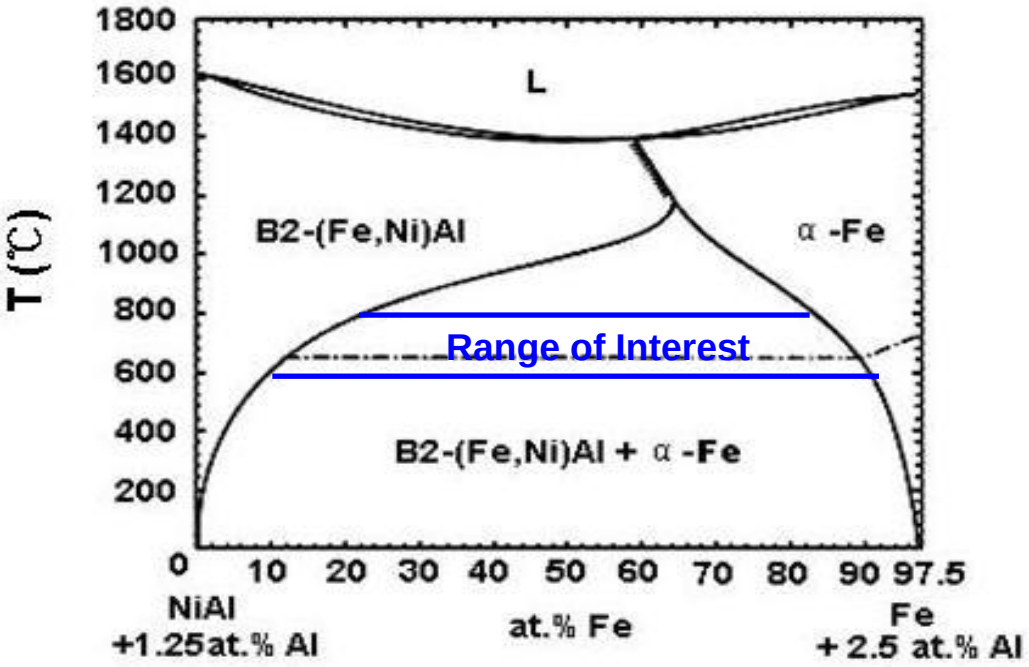

Ordered B2 (Fe, Ni)Al-type and ordered $L2_1$ Ni_2TiAl-type precipitates can form in a coherent-coplanar orientation, providing the possibility of achieving a Fe-based analogue to the Ni-based superalloys.

Ferritic Alloys as Candidates for Steam Turbine (4)

Why B2 or/and $L2_1$ precipitates strengthened ferritic steels?

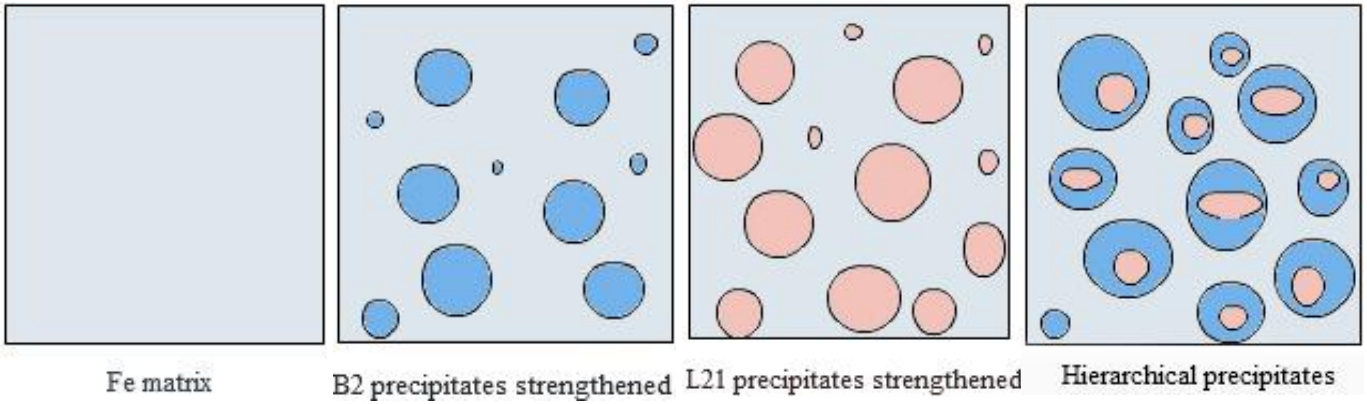

- The elevated-temperature strength of NiAl-type precipitates is limited by their properties.
- The creep strength (defined as the stress to maintain a steady-state rate of 10^{-7} s^{-1}) of Ni_2TiAl between 1, 026 to 1, 273 K is about three times that of NiAl in its most creep-resistant form.
- The creep strength of NiAl-Ni_2TiAl two-phase alloys are more creep resistant than either of the phases in its monolithic form and at least comparable to the Ni-based superalloy, MAR-M200 (nominal composition wt.%: Cr 9.0; Co 10.0; W 12.5; Nb 1.0; Ti 2.0; Al 5.0; C 0.15; B 0.015; Ni balance).

P. R. Strutt, R. S. Polvani, and J. C. Ingram. Metallurgical Transaction A. 7, 23 (1976)
R. S. Polvani, W. S.Tzeng, and P. R. Strutt. Metallurgical Transaction A. 7, 33 (1976)

Ferritic Superalloys as a Materials System

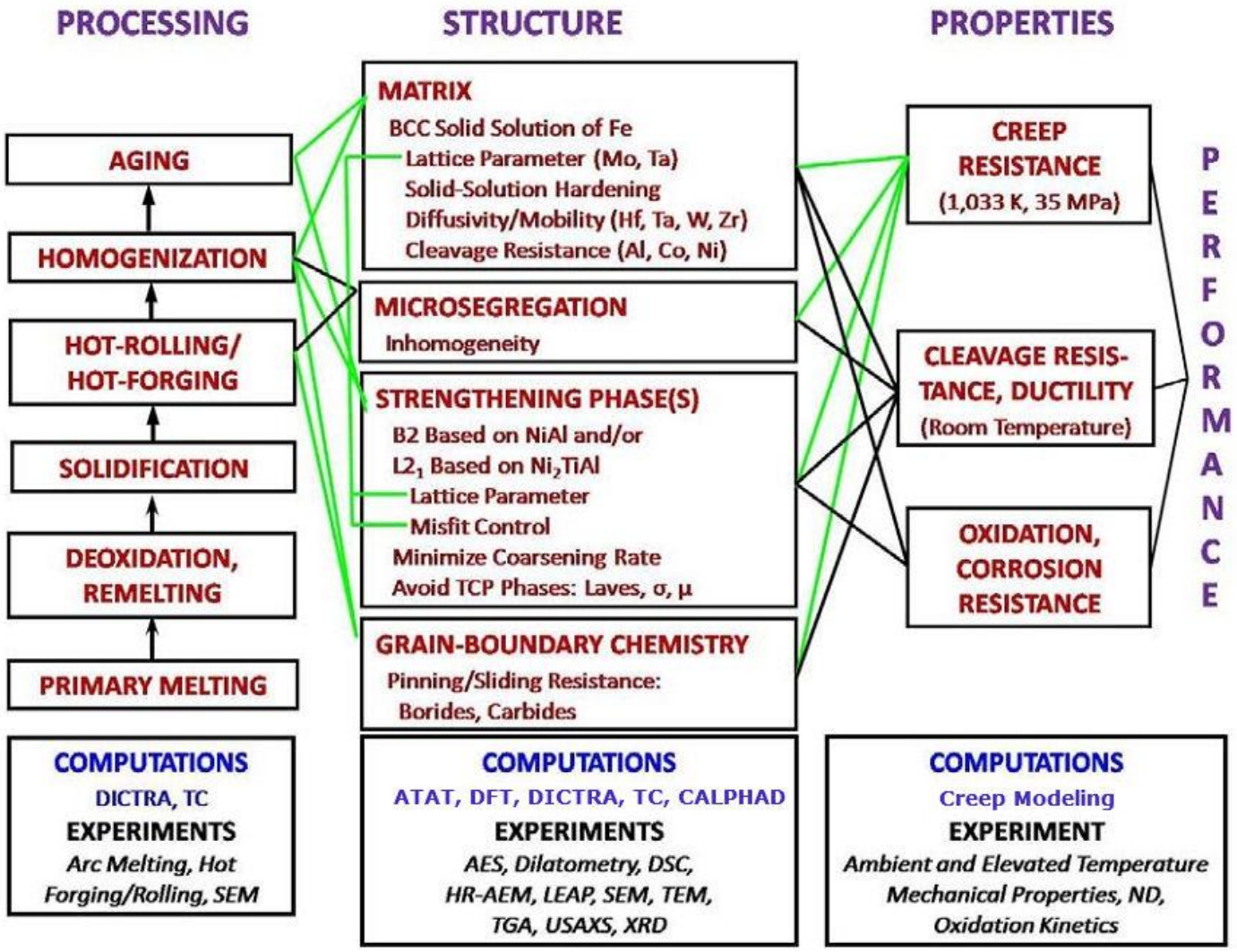

TC: Thermo-Calc; DICTRA: DIffusion Controlled TRAnsformations; DFT: Density Functional Theory; ATAT: Alloy Theoretic Automated Toolkit; CALPHAD: Calculation of Phase Diagrams; HR-AEM: High-Resolution Analytical Electron Microscope; LEAP: Local Electrode Atom Probe; SEM/TEM: Scanning/Transmission Electron Microscope; TGA: Themo-Gravimetric Analysis; USAXS: Ultra-Small-Angle X-ray Scattering; XRD: X-ray Diffraction

Potential Significance of the Results of the Work

Relevance and Outcomes/Impacts

- The proposed research will advance computational modeling used in the accelerated design of high-temperature alloys.
  - The establishment of robust computational tools and algorithms to assist alloy design and optimization.
  - Computational thermodynamic and kinetic quantities from first-principles calculations, applicable to many other high-temperature alloy systems.
  - Quantitative creep modeling for designing a wide range of advanced precipitation-strengthened alloys.
  - The development of a novel creep-resistant hierarchical ferritic superalloys
  - The training of Ph.D. students and research associates

Statement of Project Objectives

Project Objectives

- **Objective 1:** to develop and integrate modern computational tools and algorithms required to assist in the optimization of creep properties of high-temperature alloys for fossil-energy applications
  - Integrate tools and methods associated with predictive first-principles calculations, computational thermodynamic and kinetic modeling, and meso-scale dislocation-dynamics simulations.
- **Objective 2:** to achieve a fundamental understanding of the processing-microstructure-property-performance links underlying the creep behavior of novel ferritic superalloys strengthened by *B2 and/or* $L2_1$ intermetallics.
  - validate some of the computational results by measuring selected microstructural attributes in representative model ferritic superalloys with a hierarchical microstructure

Project Tasks

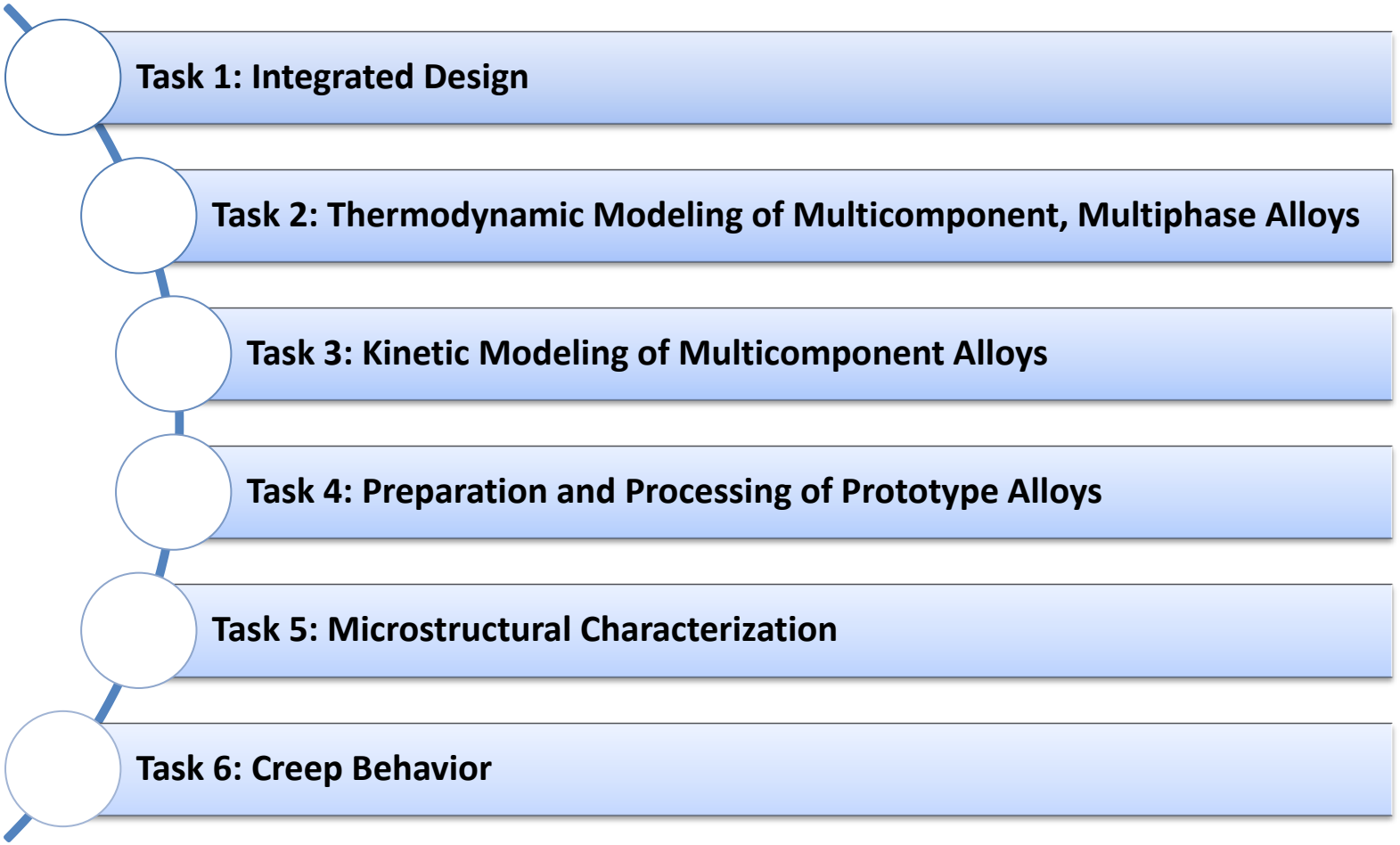

The Project Team

Role of Participants (1)

PI: Peter K. Liaw of University of Tennessee

- Manage the overall research program, formulate the research plan, monitor all aspects of the research, and supervise the graduate students.
- Lead the design and fabrication of alloys
- Contribute in the microstructure and creep study by neutron and synchrotron techniques

Co-PI: Mark D. Asta of University of California, Berkeley

- Lead the kinetic modeling of multicomponent alloys by first-principles methods.
- Collaborate with Prof. Ghosh in the integration of modeling efforts and development of tools and algorithms.

Co-PI: Gautam Ghosh of Northwestern University

- Lead the integration of modeling and development of new simulation algorithms
- Contribute to the microstructural characterizations

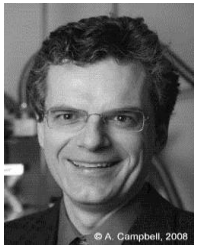

Co-PI: David Dunand of Northwestern University

- Lead the creep-behavior investigations using combined experimental methods and theoretical dislocation-dynamics simulations

Role of Participants (2)

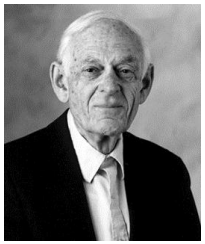

Consultant: Morris E. Fine of Northwestern University, Member of National Academy of Engineering

- Provide insight and knowledge on the alloy design, mechanical behaviors, and precipitation strengthening.

Consultant: Chain T. Liu of Hong Kong Polytechnic University / Auburn University, Member of National Academy of Engineering

- Provide technical comments in alloy design and other metallurgical aspects.

Collaborator: Ulrich Dahmen of the National Center for Electron Microscopy

- Perform electron-microscopy studies to validate the computational models

Collaborator: Velimir Radmilovic of the National Center for Electron Microscopy

- Perform and mentor a postdoctoral fellow in electron-microscopy measurements

Role of Participants (3)

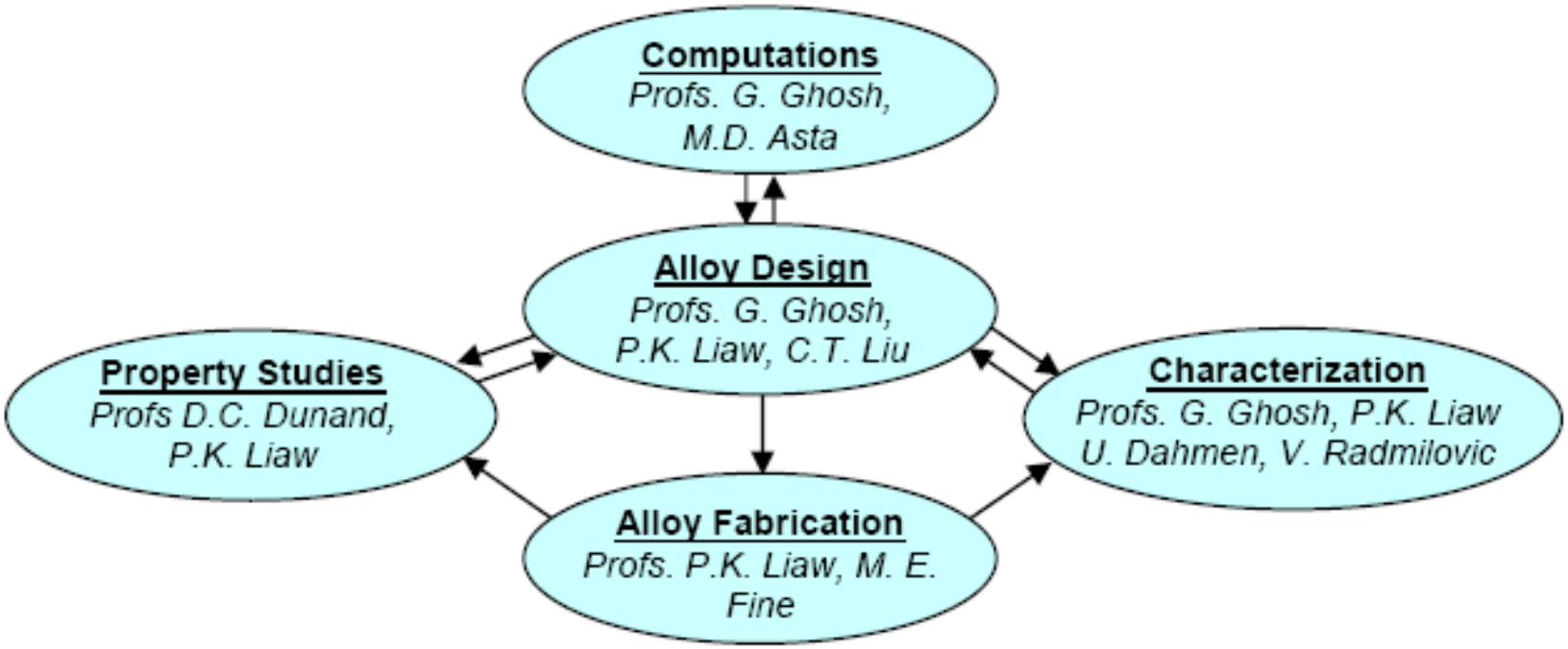

Schematic flow chart illustrating the roles of the participants and the integration of the activities in the computation-based alloy-design project

Prof. Ghosh's Presentation
Previous Results

Conceptual Microstructures (1)

- Dispersion of NiAl-type precipitates in an Fe matrix

TEM BF showing coherency strain contrast

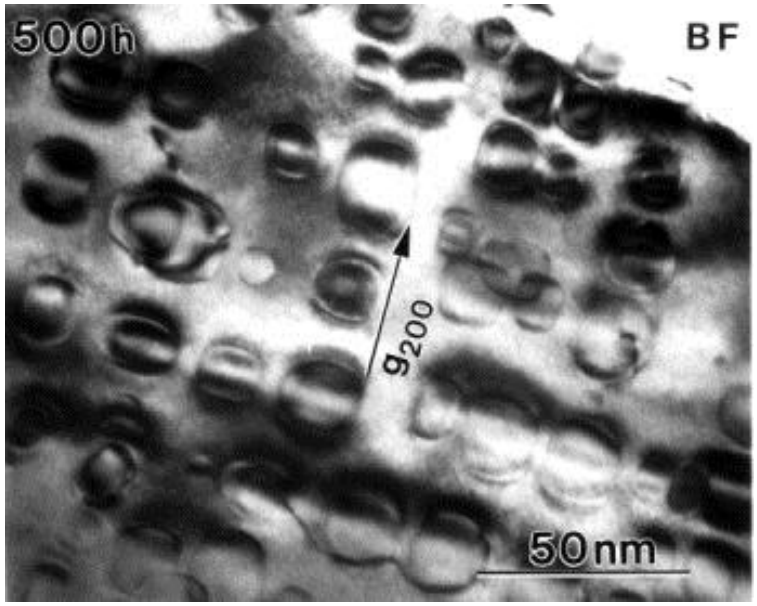

TEM DF (using 100-type reflections) showing B2 precipitates

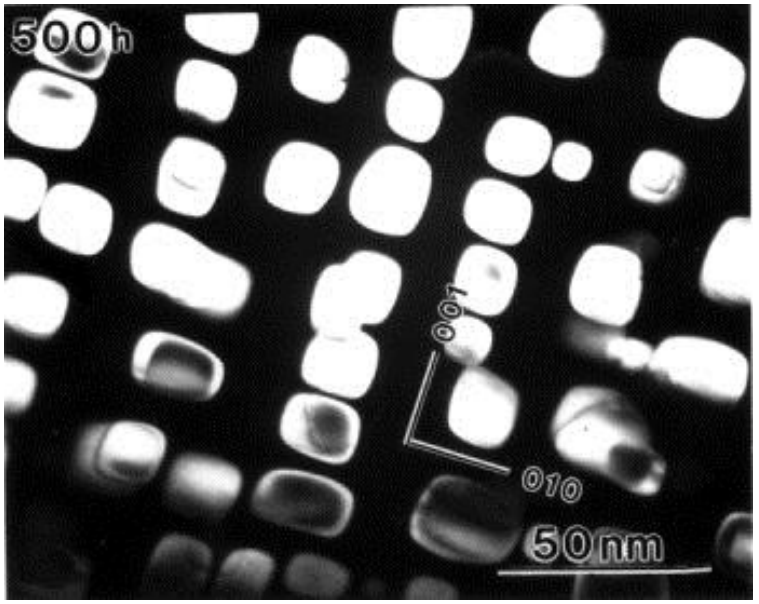

Alloy composition: Fe-8.08Al-12.2 Cr-1.9Mo-18.2Ni (wt. %)

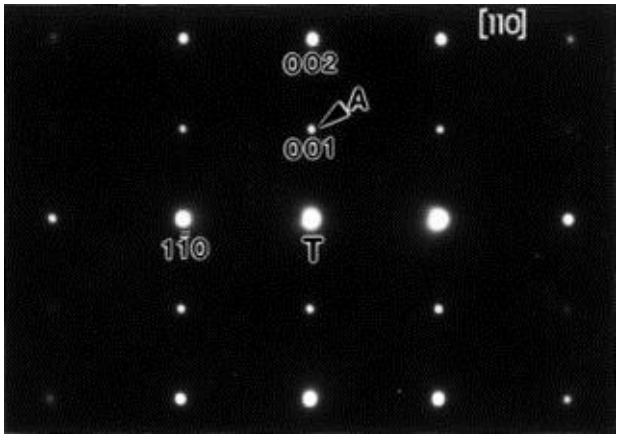

G. Ghosh, Unpublished research, NU

Conceptual Microstructures (2)

- Dispersion of Ni_2TiAl-type $L2_1$ precipitates in an Fe matrix

TEM DF (using 100-type reflections)
Common to both *B*2 and $L2_1$ structures

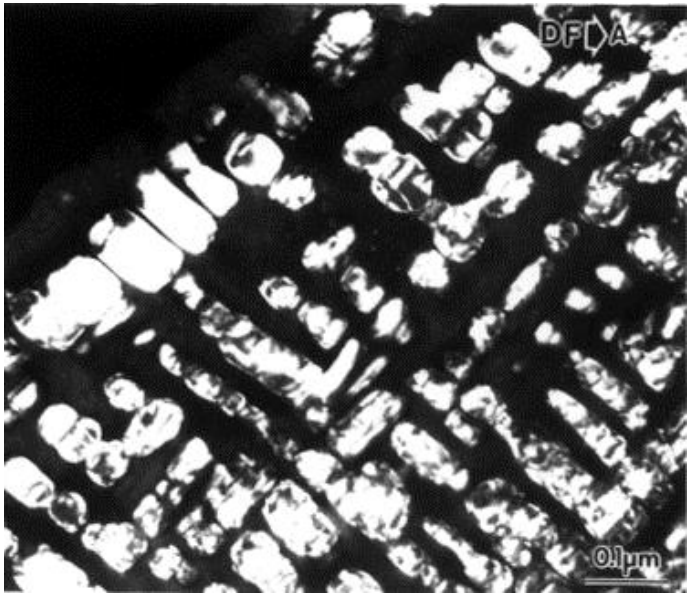

TEM DP showing reflections of both
*B*2 and $L2_1$ type structures

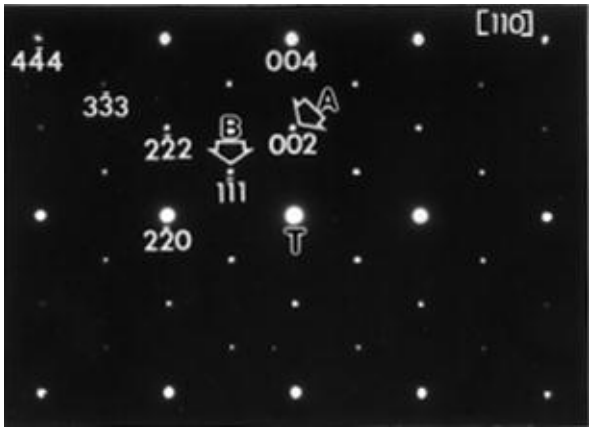

TEM DF (using 111-type reflections)
Unique to $L2_1$ structures

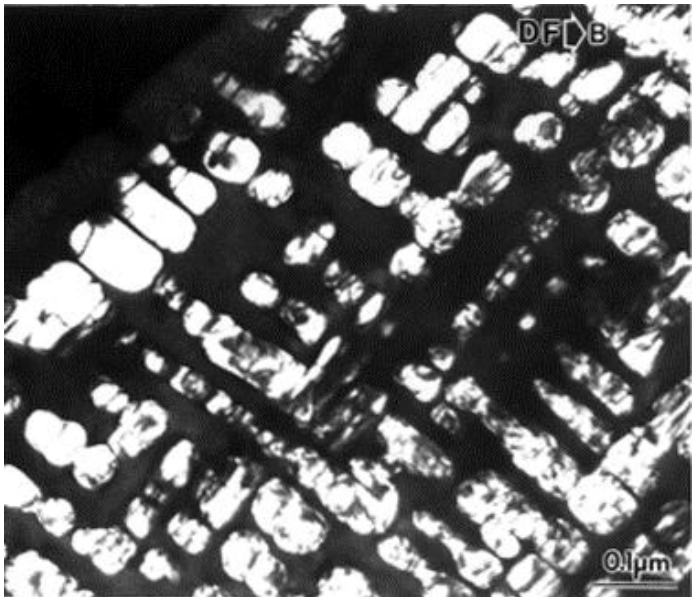

Alloy composition: Fe-8.08Al-12.2 Cr-1.9Mo-18.2Ni-6Ti (wt. %)

G. Ghosh, Unpublished research, NU

Conceptual Microstructures (3)

- A hierarchical microstructure: NiAl-type and Ni_2TiAl-type precipitates

TEM BF micrograph

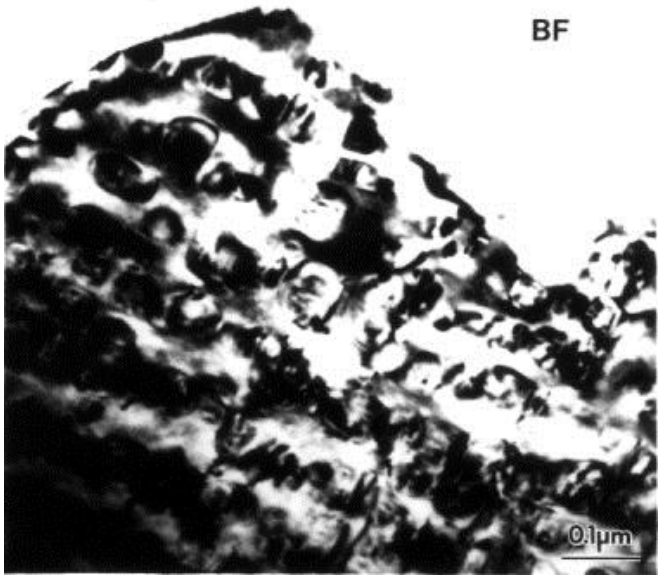

TEM DP showing reflections of both *B*2 and $L2_1$ type structures

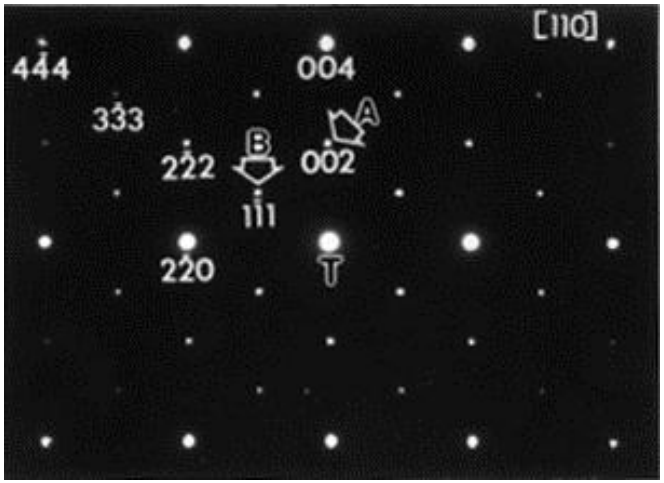

Alloy composition: Fe-8.08Al-12.2Cr-1.9Mo-18.2Ni-2Ti (wt. %)

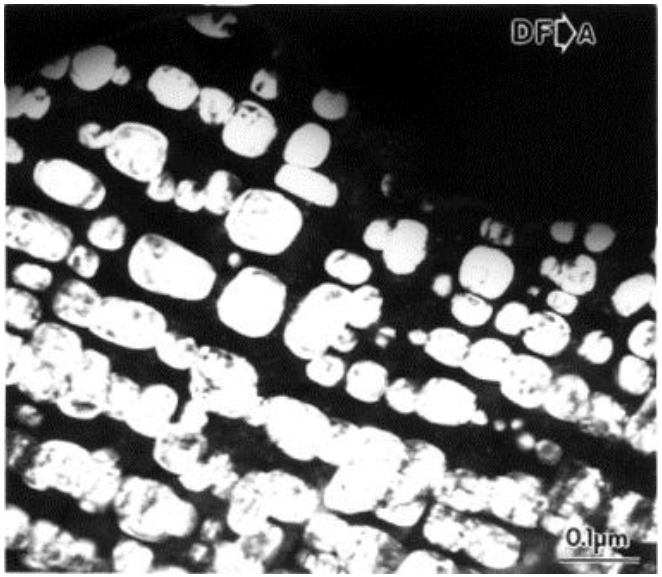

TEM DF using (200)-type $B2/L2_1$ spots

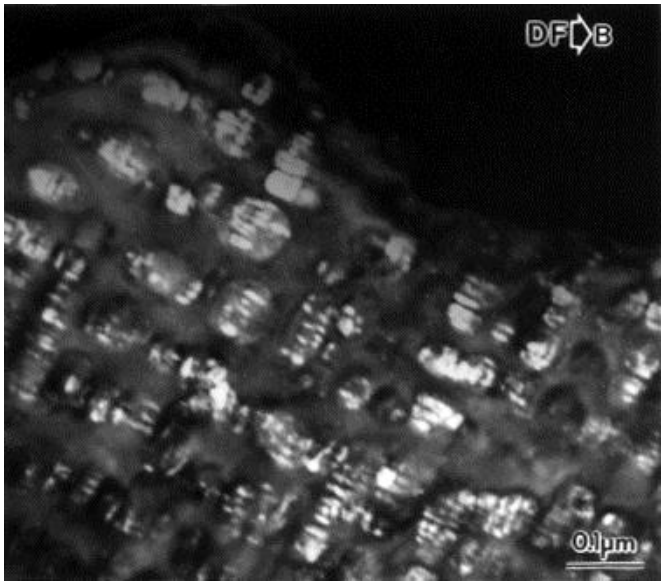

TEM DF using (111)-type $L2_1$ spots (unique)

G. Ghosh, Unpublished research, NU

Calculation of Coherent Interfacial Energies (1)

- Sharp Interface Models
  - Construction of structural models (supercells) followed by total energy calculation from first-principles
- Diffuse Interface Models
  - Cluster expansion followed by Monte Carlo simulations
  - In progress

- **Supercell Method (Sharp Interface):**
  - **Supercells of different sizes are constructed with {100}, {110} and {111} habits. Supercells are gradually increased in a direction perpendicular to the habit plane**
  - **Convergence of the calculated interfacial energy is checked w.r.t. the supercell size**
  - **Calculated interfacial energy (γ) is defined as**

$$\gamma = (E_{Fe/B2}[n_{Fe}, n_{B2}] - 0.5(E_{Fe}[2n_{Fe}] + E_{B2}[2n_{B2}]))/2A$$

where the supercell contains *n* unit cells of Fe (n_{Fe}) and *B2* (n_{B2}) phases, *E* is the corresponding total energy and *A* is the interfacial area interfacial energy

Calculation of Coherent Interfacial Energies (2)

- Structural models for bcc-Fe and B2-NiAl with an interface

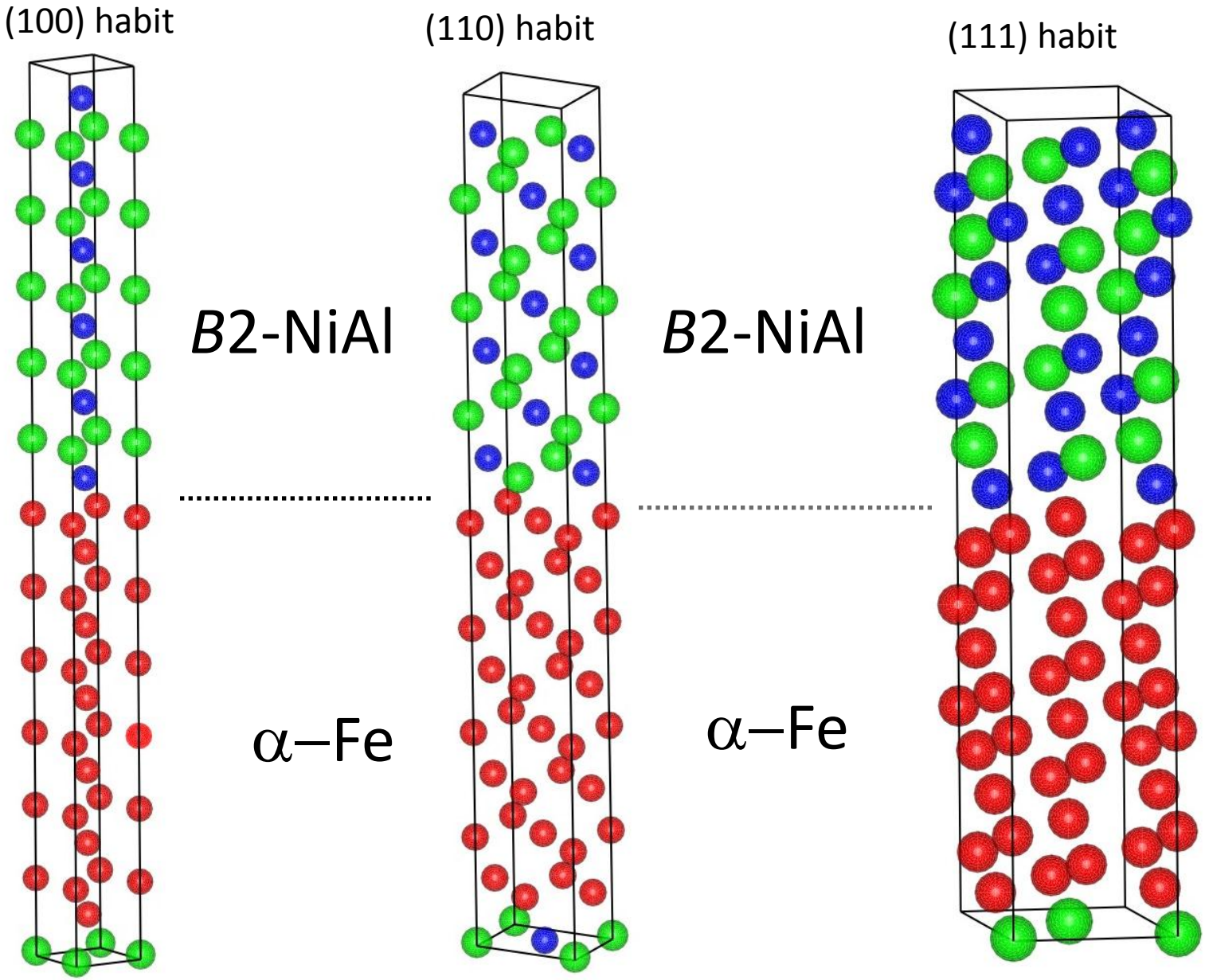

Calculation of Coherent Interfacial Energies (3)

- A systematic study of bcc-Fe and *B*2: Case Fe/*B*2-FeAl

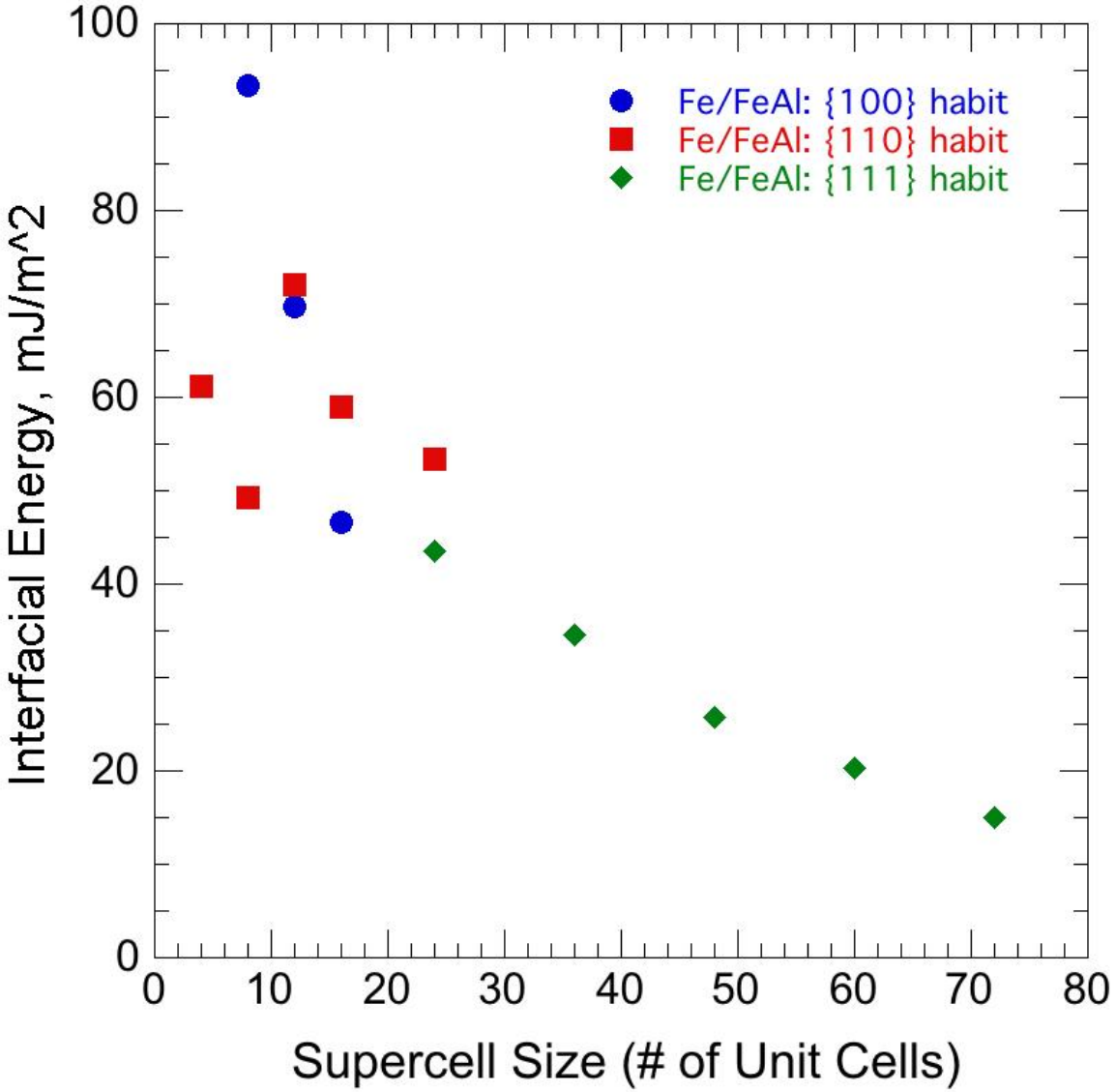

Calculation of Coherent Interfacial Energies (4)

- A systematic study of bcc-Fe and *B*2: Case Fe/*B*2-CoAl

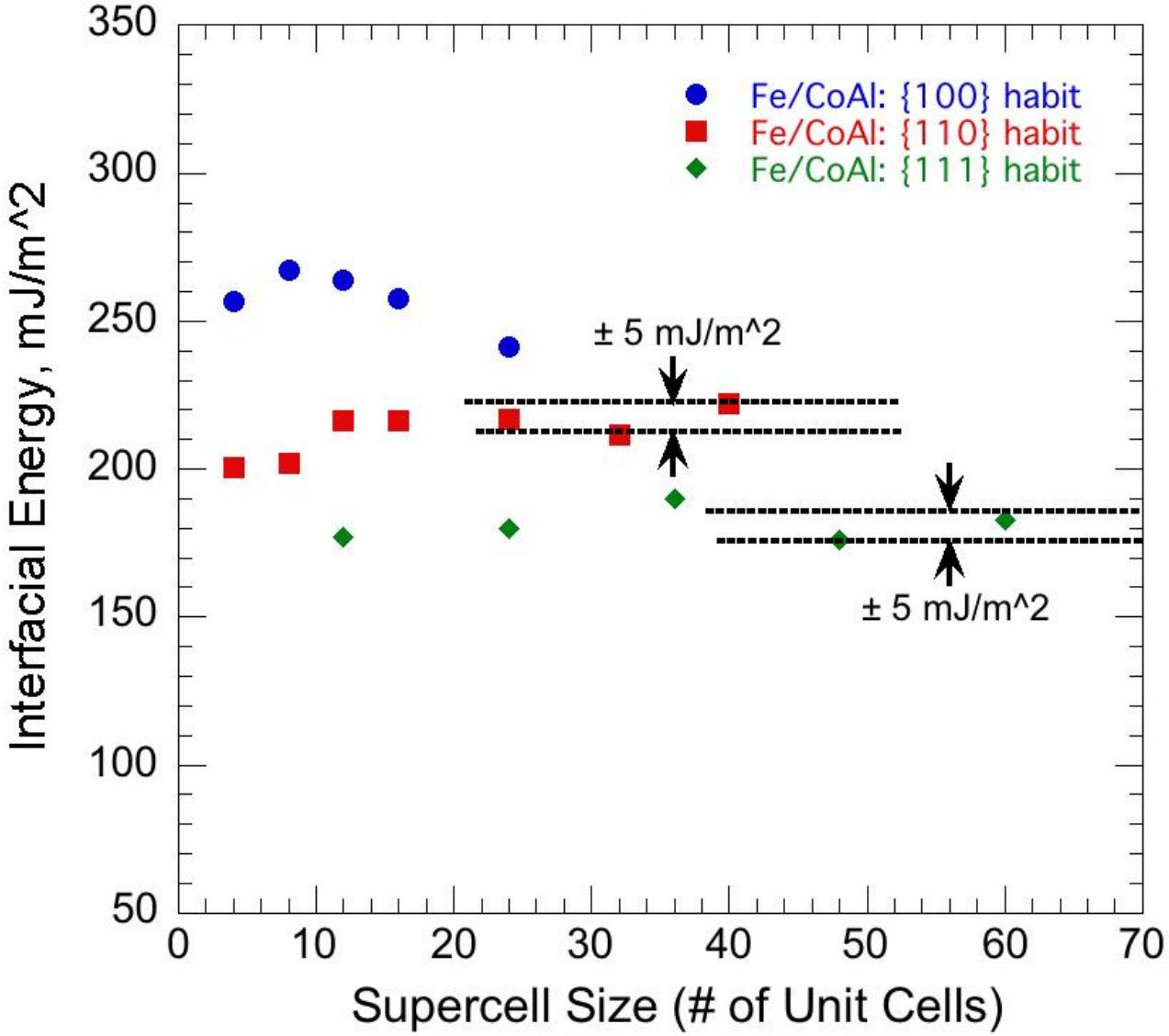

Calculation of Coherent Interfacial Energies (5)

- A systematic study of bcc-Fe and *B*2: Fe/*B*2-NiAl

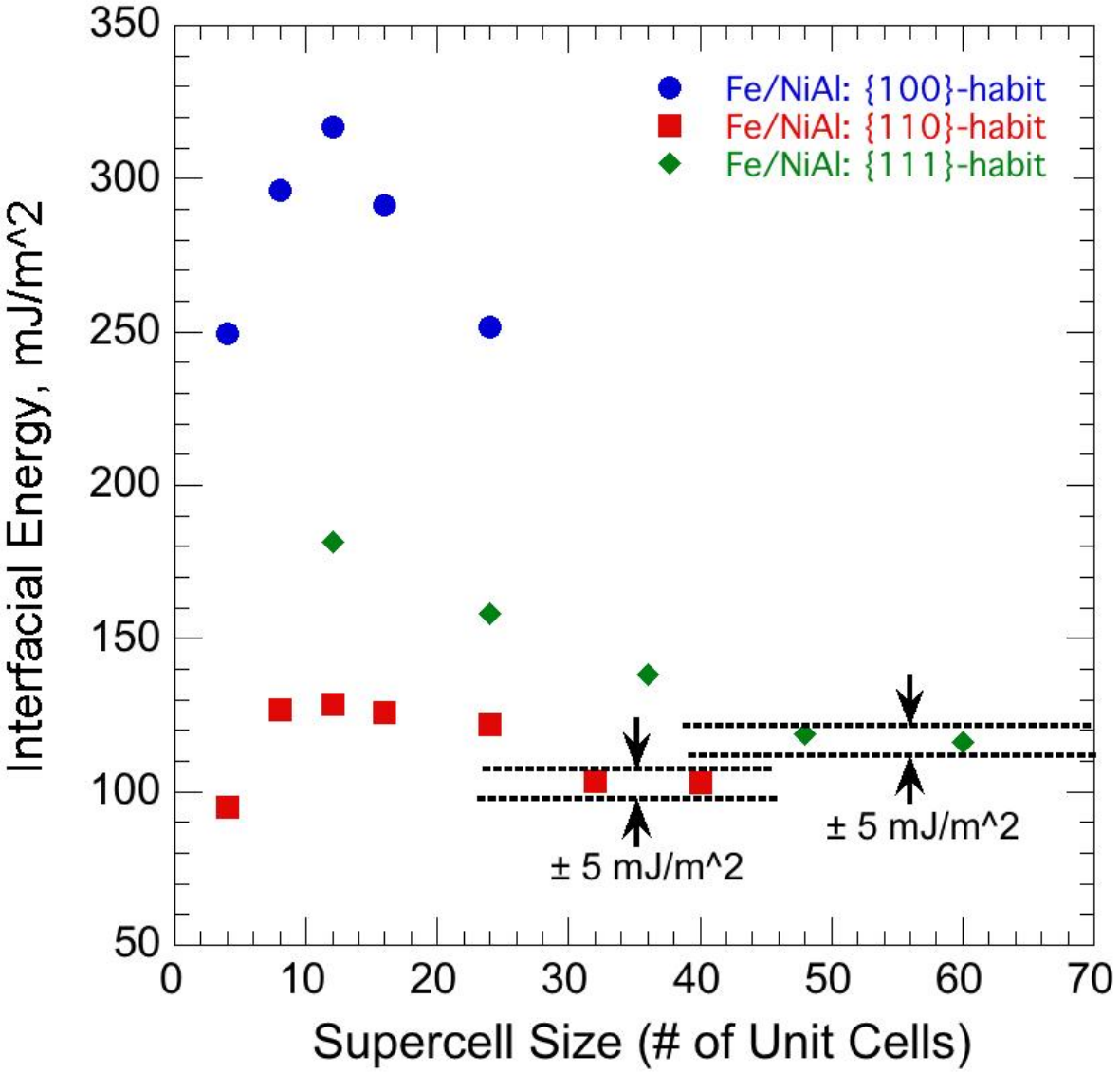

Proposed Research and Detailed Technical Approach to Achieve the Project Goals

Integrated Computational Approach

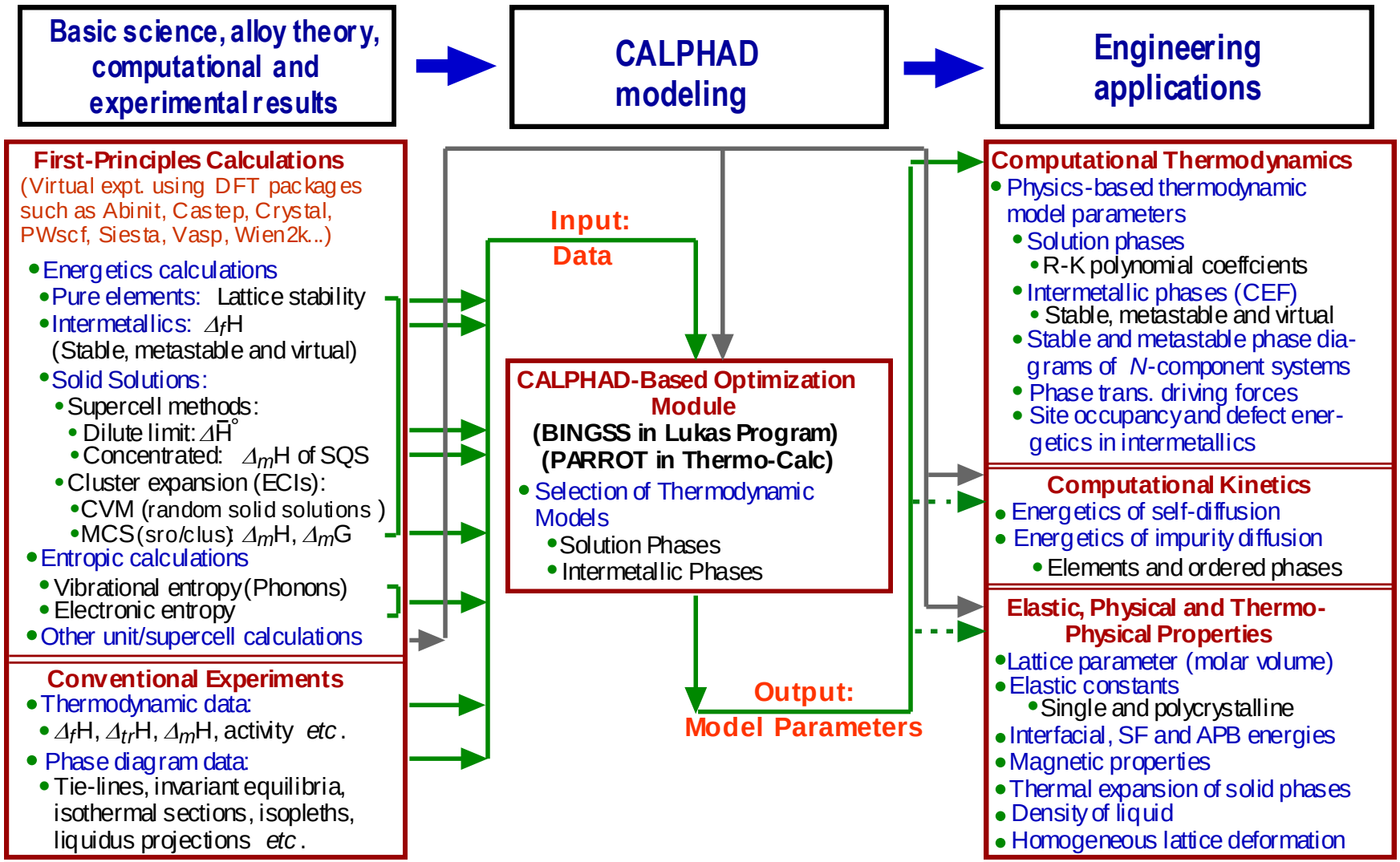

G. Ghosh, A. van de Walle, M. Asta, Acta Mater., 56, 3202 (2008)

Proposed Research

- Principal computational tools
  - Vienna Ab-initio Simulation Package (VASP): total energy and electronic structures
  - Alloy Theoretic Automated Toolkit (ATAT): cluster expansion (energy, lattice parameter, elastic properties of disordered solid solutions), Monte Carlo simulation (diffuse interface energy)
  - Thermo-Calc: multi-component, multi-phase equilibria
    - Predictive accuracy depends on the accuracy of database
  - DICTRA: multi-component, multi-phase diffusion
    - Predictive accuracy depends on the accuracy of database
- Hardware resources
  - QUEST cluster (NU)
  - TeraGrid resources
  - NERSC resources (Lawrence Berkeley National Laboratory)

Proposed Research

- Cluster expansion (formation energy bcc solid solutions)
  - VASP + ATAT results define effective cluster interaction (ECIs) parameters
  - There may not be a bcc solid solution in the equilibrium phase diagram (e.g., bcc phase field in the Ni-Al system)!

bcc Al-Ni

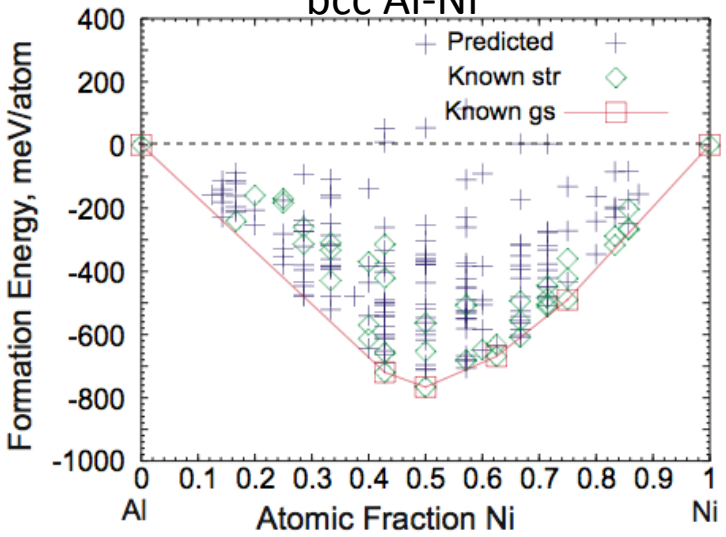

bcc Fe-Ni

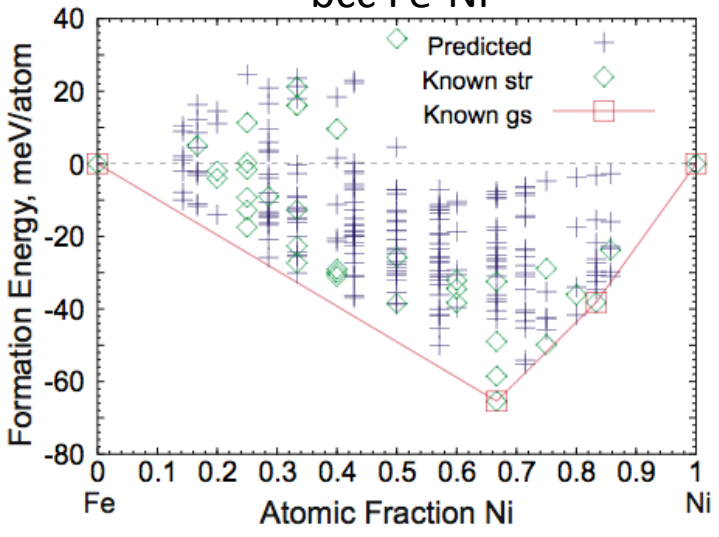

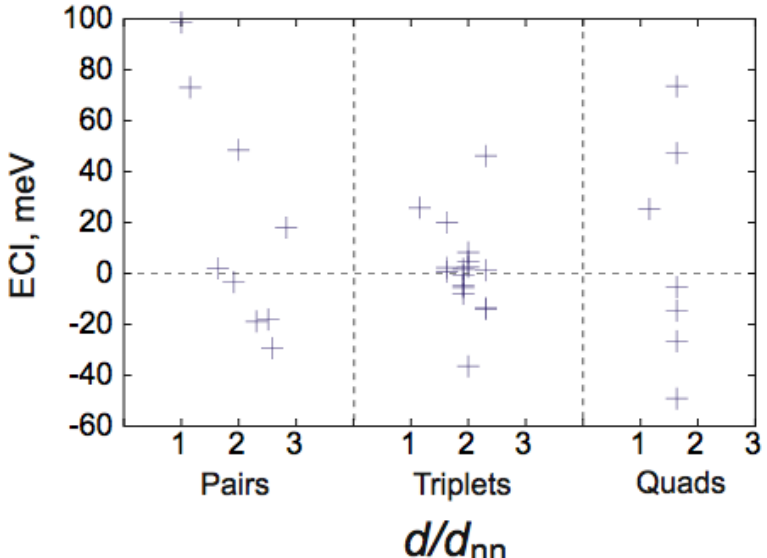

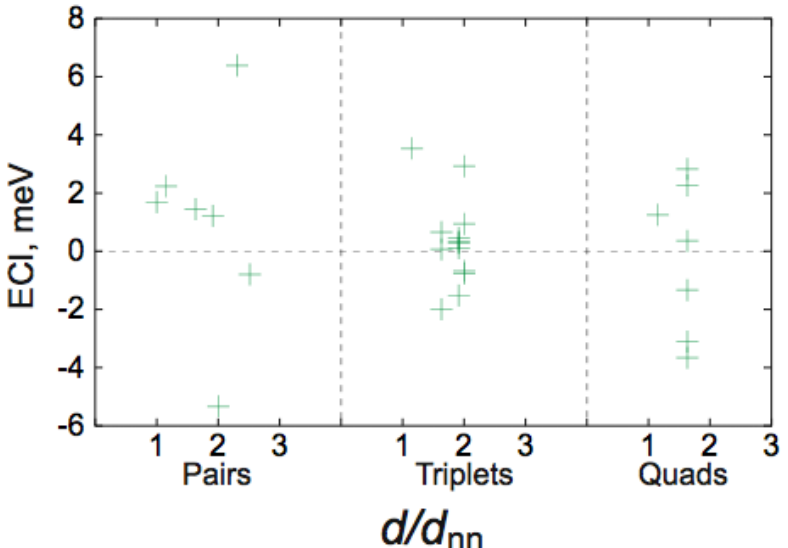

Proposed Research

- Interfacial energy calculations
  - Sharp interface models: additional calculations using larger supercells are needed to ensure converged results
  - Diffuse interface models: Cluster expansion followed by Monte Carlo simulations will be carried out, and results will be compared with those obtained from sharp interface models

- Composition dependence of elastic constants
  - Analogous to energetics of solid solutions, a cluster-expansion method will be employed to compute the composition dependence of elastic constants (C_{ij}) solid solutions
  - Systems of interest: Fe-Al, Fe-Cr, Fe-Ni, and Al-Ni
  - Elastic constants (C_{ij}) of intermetallics: relevant $B2$ and $L_2 1$

Proposed Research

- Integration of first-principles results
  - Thermo-Calc: multi-component, multi-phase equilibria
  - Thermo-Calc: solid solutions, ordered phase with homogeneity range, ordering energies
    - Predictive accuracy depends on that of database
  - DICTRA: multi-component, multi-phase diffusion
    - Predictive accuracy depends on that of database

Prof. Asta's Presentation
Previous Results

Diffusivity Calculation by First Principles

Compilation of Published Measurements at T=1050 K

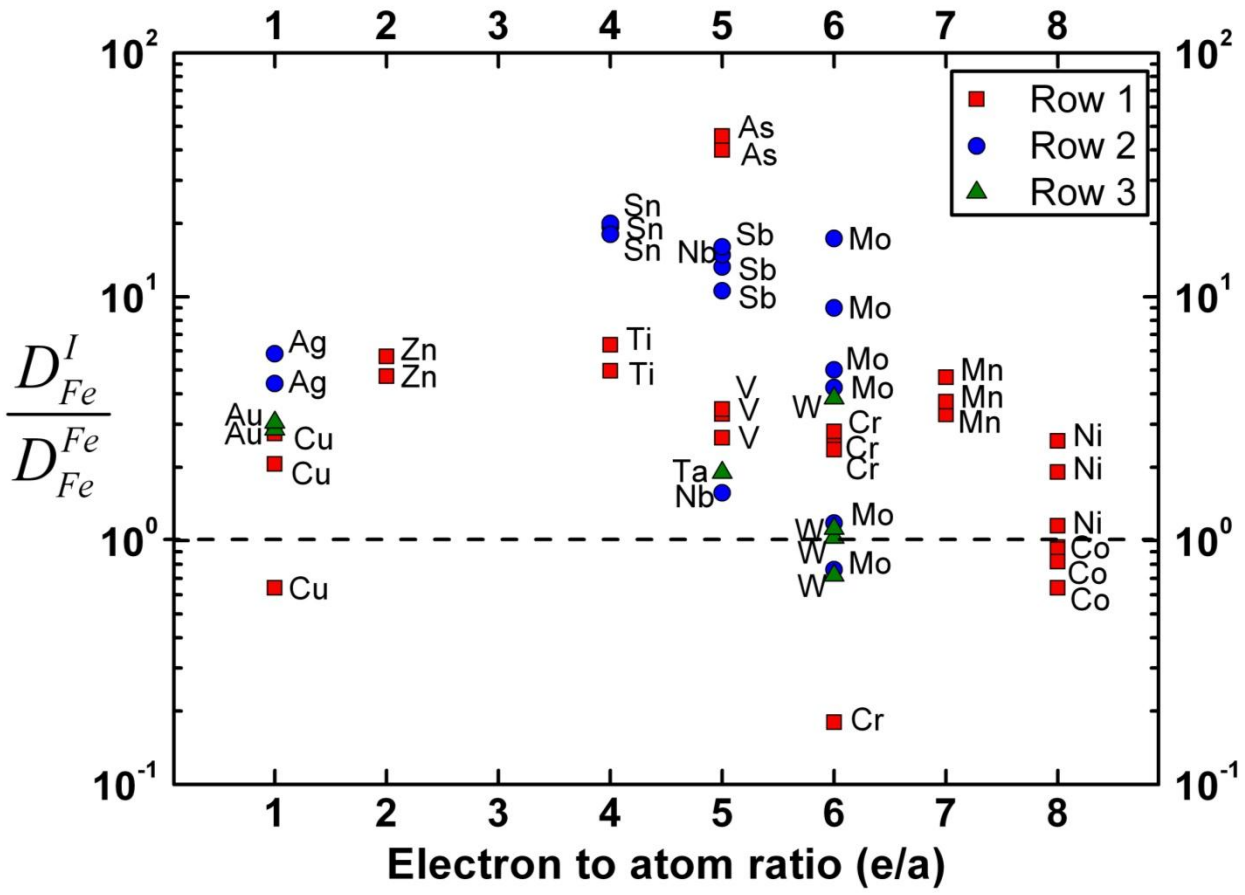

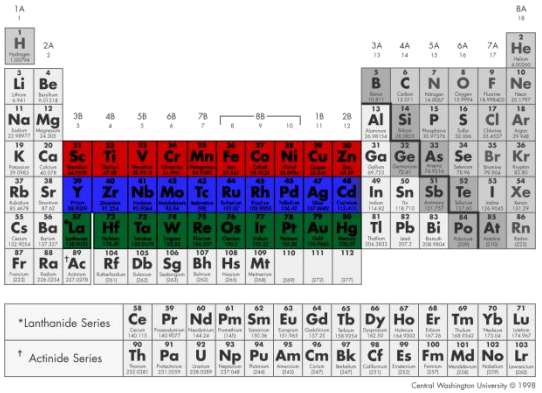

Adopted from S. Huang, D. L. Worthington, M. Asta, V. Ozolins, G. Ghosh, and P. K. Liaw. Acta Mater. 58, 1982 (2010).

- Wide Scatter in Published Data for Several Solutes
- Data Lacking for Most 5d Solutes
- Absence of Clear Slow Diffusers in Measured Data

Calculated and Experimental Results (1)

Temperature Dependence of α-Fe Self Diffusivities

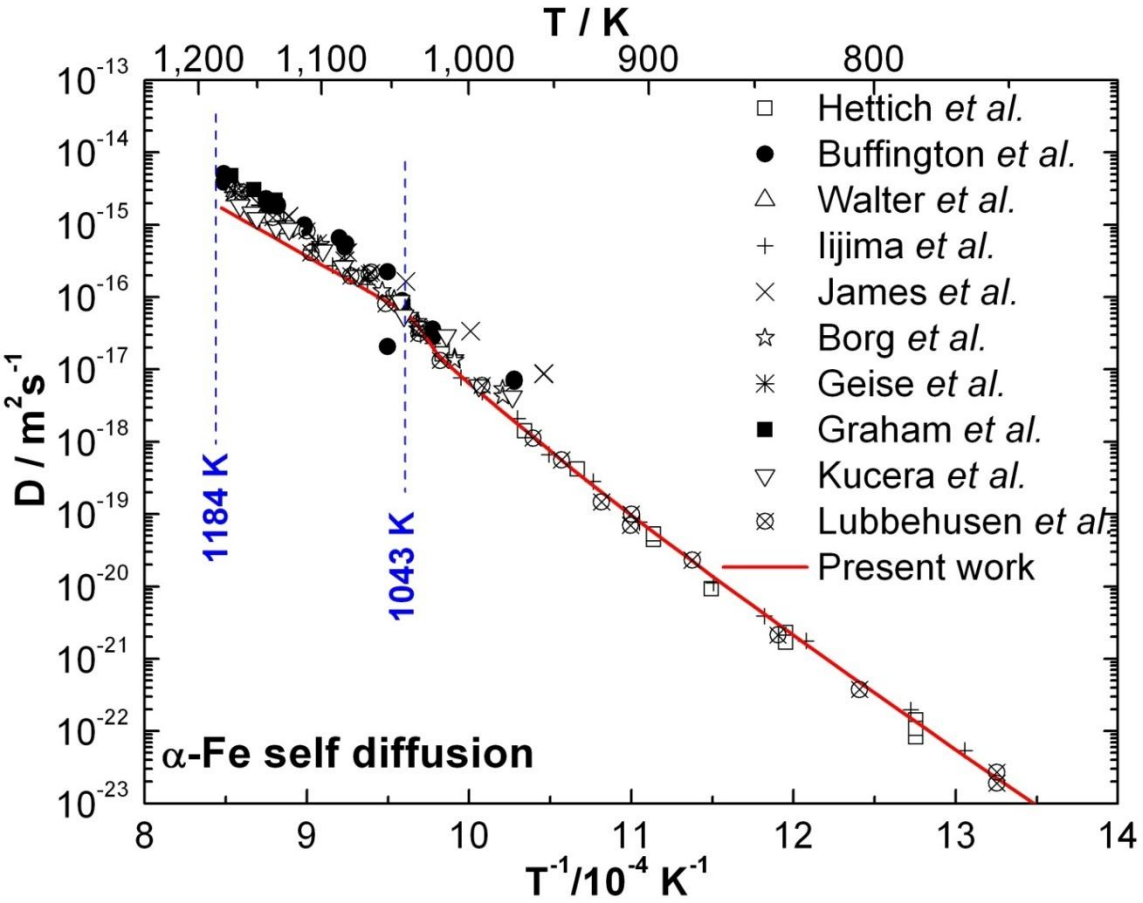

Adopted from S. Huang, D. L. Worthington, M. Asta, V. Ozolins, G. Ghosh, and P. K. Liaw. Acta Mater. 58, 1982 (2010).

[1] R. J. Borg and C. E. Birchenall, Trans. Metall. Soc. A.I.M.E. 218, 980 (1960)
[2] F. S. Buffington, K. Hirano, and M. Cohen. Acta metall. 9, 434 (1961)
[3] G. Hettich, H. Mehrer, and K. Maier, Script0 metoll. 11, 795 (1977)
[4] C. M. Walter and N. L. Peterson, Phys. Rer. 178, 922 (1969)
[5] D. W. James and G. M. Leak, Phil. Mag. 14, 701 (1966)
[6] Y. Iijima, K. Kimura ,and K. Hirano, Acta Met., 36, 2811 (1988)
[7] J. Geise and Ch. Herzig, Z. Metallk. 78, 291 (1987)
[8] D. Graham and D. H. Tomlin, Phil. Mag. 8, 1581 (1963)
[9] M. Lübbehusen and H. Mehrer, Acta Metall. Mater. 38, 283 (1990)
[10] J. Kucera, B. Millien, J. Ruzickova, V. Foldyna and A. Jakobova. Acta Met. 22, 135 (1974)

Calculated and Experimental Results (2)

Temperature Dependence of W Impurity Diffusivities

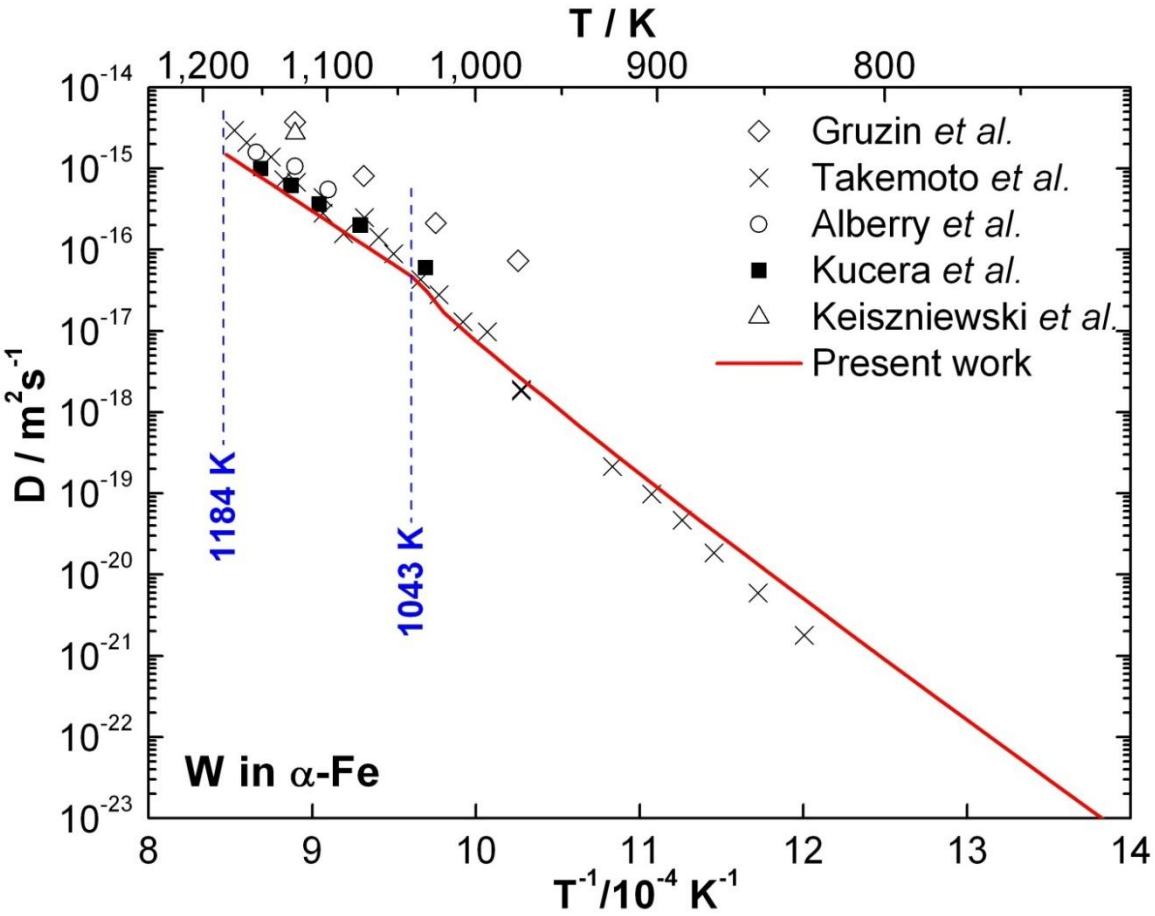

Adopted from S. Huang, D. L. Worthington, M. Asta, V. Ozolins, G. Ghosh, and P. K. Liaw. Acta Mater. 58, 1982 (2010).

[1] P. L. Gruzin, Dokl. Akad. Nauk. SSSR 94 681 (1954).
[2] J. Kieszniewski, Pr. Inst. Hutn. 19 253 (1967).
[3] J. Kucera, B. Million, and K. Ciha, Kov. Mater. 7 9 (1969).
[4] P. J. Alberry and C. W. Haworth, Met. Sci. 8 1269 (1974).

Calculated and Experimental Results (3)

Temperature Dependence of Mo Impurity Diffusivities

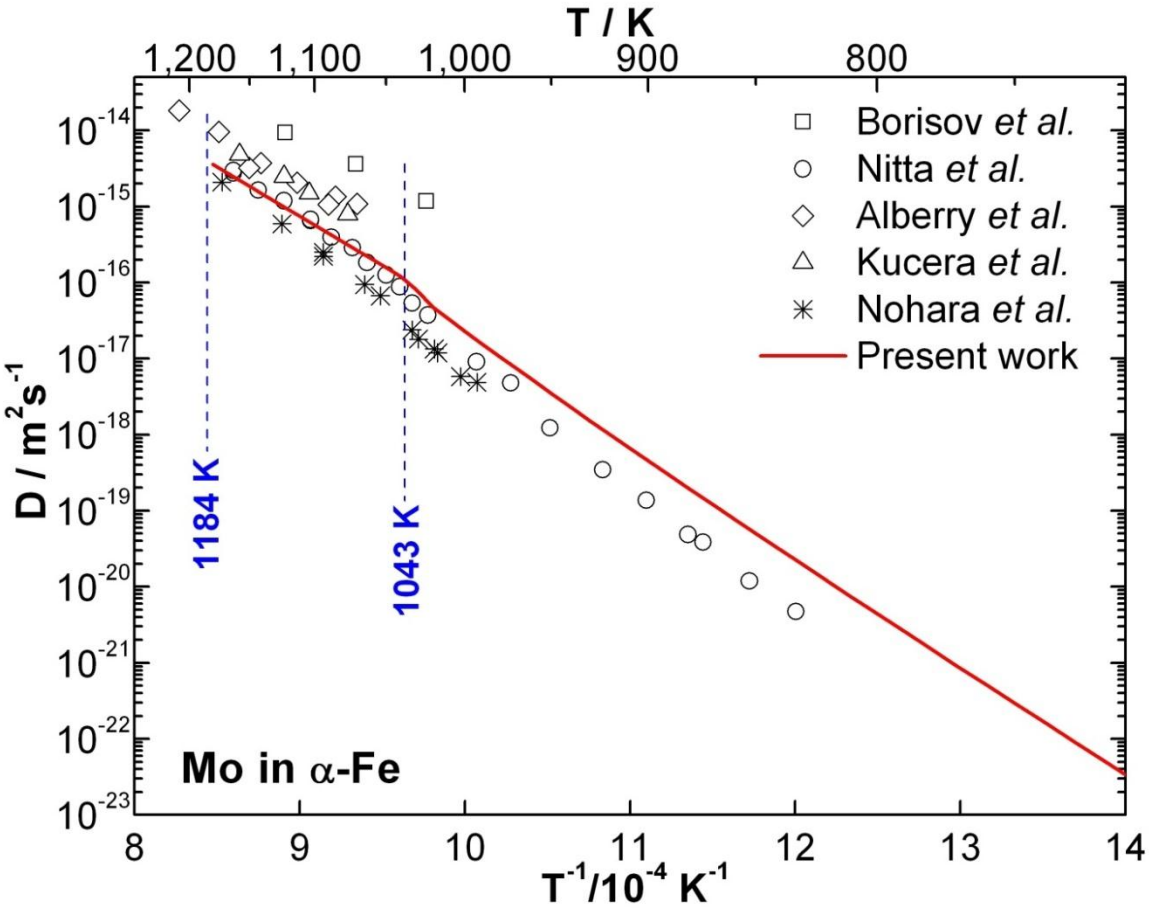

Adopted from S. Huang, D. L. Worthington, M. Asta, V. Ozolins, G. Ghosh, and P. K. Liaw. Acta Mater. 58, 1982 (2010).

[1] V. T. Borisov, V. M. Golikov, and G. V. Sherbedinskiy, Phys. Met. Metallogr. 22, 175 (1966).
[2] J. Kucera and B. Million, K. Ciha, Kov. Mater., 7, 97, (1969).
[3] K. Nohara and K. Hirano, J. Japan Inst. Met. 40, 407, (1976).
[4] P. J. Alberry and C. W. Haworth, Met. Sci., 8,1269 (1974).
[5] H. Nitta, Acta Materialia, 50, 4117-4125 (2002).

Proposed Research and Detailed Technical Approach to Achieve the Project Goals

Model for Self and Impurity Diffusivities

Harmonic Transition State Theory Assuming Vacancy Mechanism

$$D_A^B = D_{0A}^B \exp[-Q_A^B / k_B T]$$

Self Diffusion in α-Fe

$$D_{0Fe}^{Fe} = a^2 f_{bcc} \exp\left[\frac{\Delta S_v^f}{k_B}\right] x \left[\prod_{i=1}^{3N-3} \nu_i^{vac} \Big/ \prod_{i=1}^{3N-4} \nu_i^{sad}\right] \qquad Q_{Fe}^{Fe} = \Delta H_v^f + \Delta H_v^{mig,Fe}$$

Impurity Diffusion

$$D_{0Fe}^{I} = a^2 f_{Fe}^{I} \exp\left[\frac{\Delta S_v^f + \Delta S_v^{bind}}{k_B}\right] x \left[\prod_{i=1}^{3N-3} \nu_i^{vac} \Big/ \prod_{i=1}^{3N-4} \nu_i^{sad}\right] \qquad Q_{Fe}^{I} = \Delta H_v^f + \Delta H_v^{bind} + \Delta H_v^{mig,I}$$

Diffusivity Calculations Require Determinations of:

- Vacancy Formation, Binding and Migration Energies
- Vacancy Formation, Binding and Migration Entropies
- Correlation Factors for Impurity Diffusion

Correlation Factors

LeClaire's 9-frequency Formalism[1]

$$t_1 = -\frac{\Gamma_2}{\Gamma_2 + 3\Gamma_3 + 3\Gamma_3 + \Gamma_3 - \frac{\Gamma_3\Gamma_4}{\Gamma_4 + 0.512\times\Gamma_5} - \frac{2\Gamma_3\Gamma_4}{\Gamma_4 + 3\times 0.512\times\Gamma_0} - \frac{\Gamma_3\Gamma_4}{\Gamma_4 + 7\times 0.512\times\Gamma_0}}$$

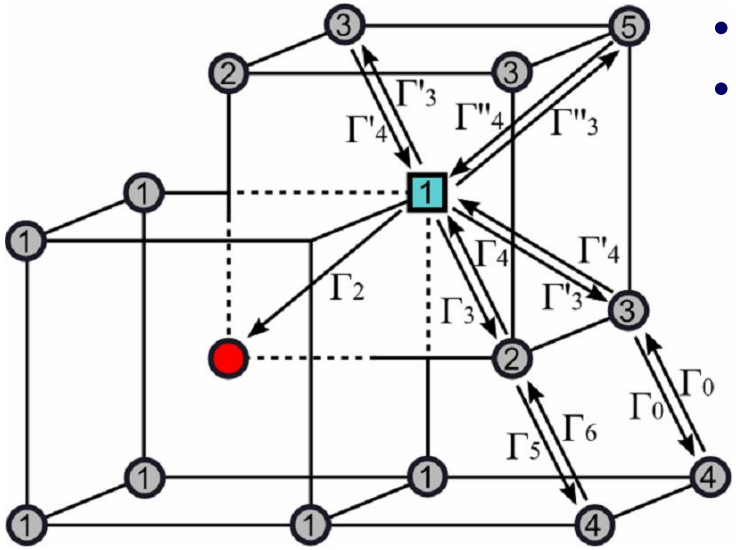

- Migration energies from 1st-principles calculations
- Attempt frequencies assumed constant

Solute	f_{solute} / f_{Fe} @ 1000 K
W	1.02
Mo	0.39
Zr	0.65
Hf	1.12

[1] A. D. Le Claire, In: H. Eyring, editor. Physical Chemistry: An Advanced Treatise, vol. 10. Academic Press (New York), 1970, chap. 5

First-Principles Calculations

- Vacancy Formation, Migration, and Binding Energies
  - VASP, PAW, Spin-Polarized GGA
  - Supercell geometries
- Entropies
  - Harmonic vibrational contributions
  - Electronic contributions included
- Saddle-Point Geometry
  - Mid-point between vacancy and solute neighbors assumed
  - Verified by nudged-elastic-band calculations for W, Fe, and Hf

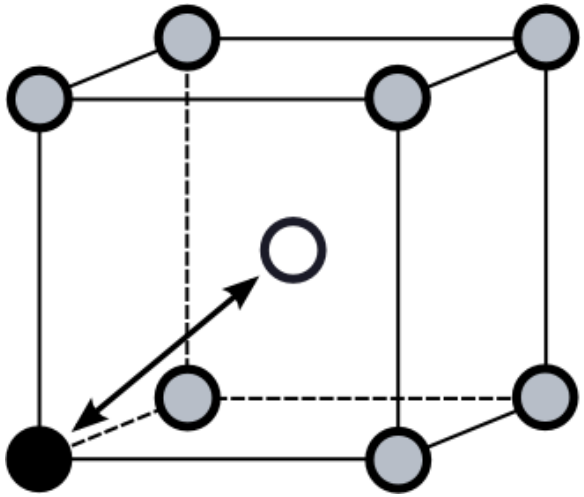

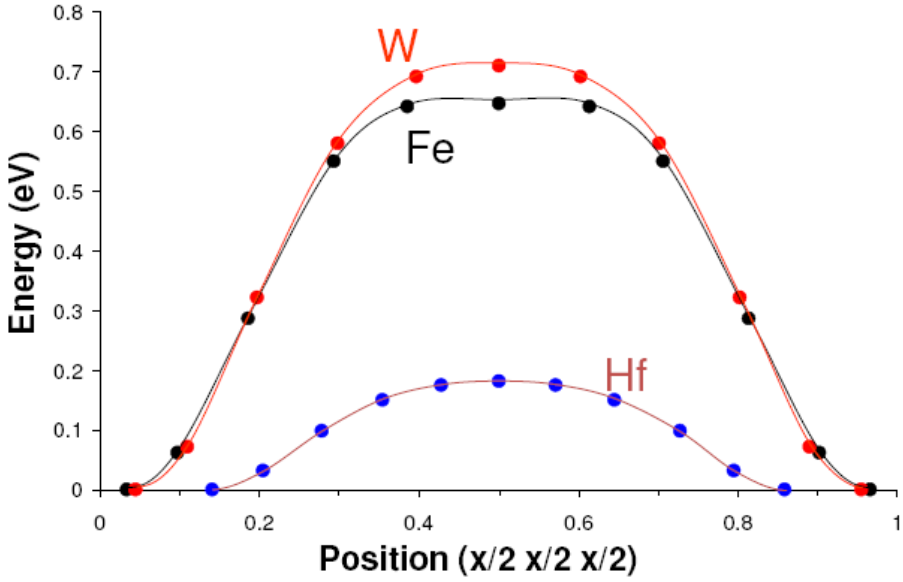

Activation Energies

Magnetic Contributions

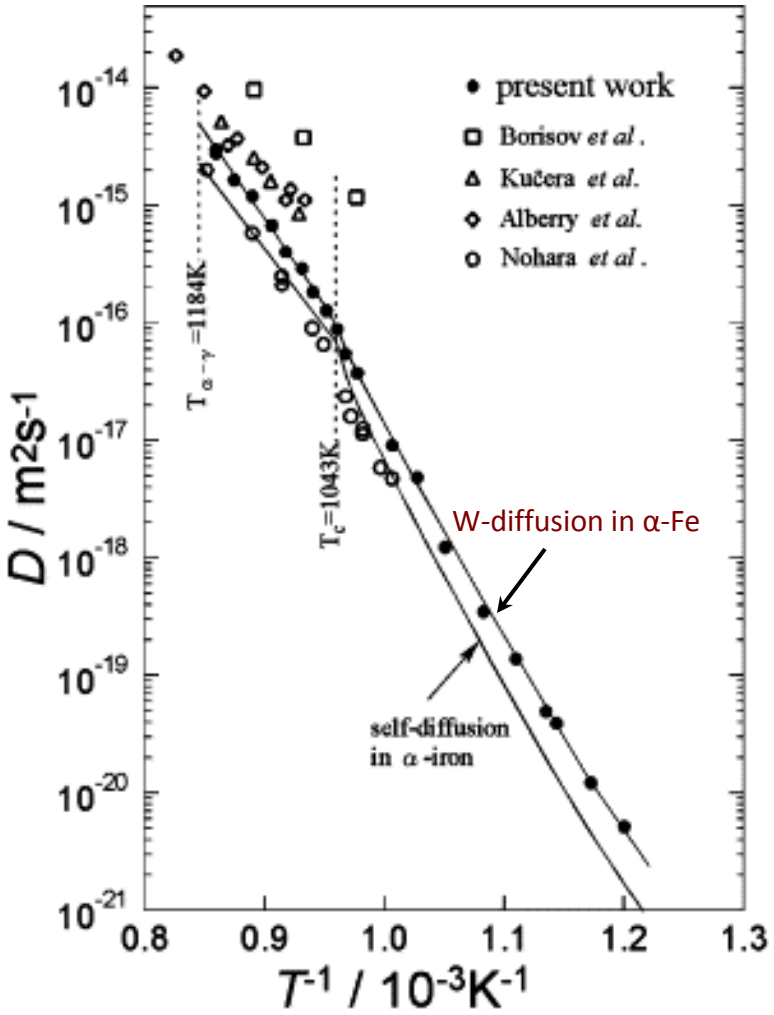

Magnetic Contribution in Ferromagnetic Phase

$$Q^F(T) = Q^P\left(1 + s(T)^2\alpha\right)$$

$$s(T) = M(T)/M(0)$$

- α quantifies the influence of magnetic ordering on activation energy, Q
- α measured for relatively few solutes

S. Takemoto, H. Nitta, Y. Iijima, and Y. Yamazaki, *Phil Mag., 2007*, v. 87, p 1619.

Semi-Empirical Model for α

Empirical Linear Relation: α and Induced Magnetization, ΔM_{12}

$$\Delta M_{12} = \sum_{i=1}^{8} \Delta m_i^{1st\ NN} + \sum_{j=1}^{6} \Delta m_j^{2nd\ NN}$$

S. Takemoto, H. Nitta, Y. Iijima, and Y. Yamazaki, *Phil Mag., 2007*, v. 87, p 1619.

- Calculate ΔM_{12} for solutes with known α
- Fit linear relationship:

$$\alpha = 0.0586\Delta M_{12} + 0.1591$$

- Predict α for other solutes

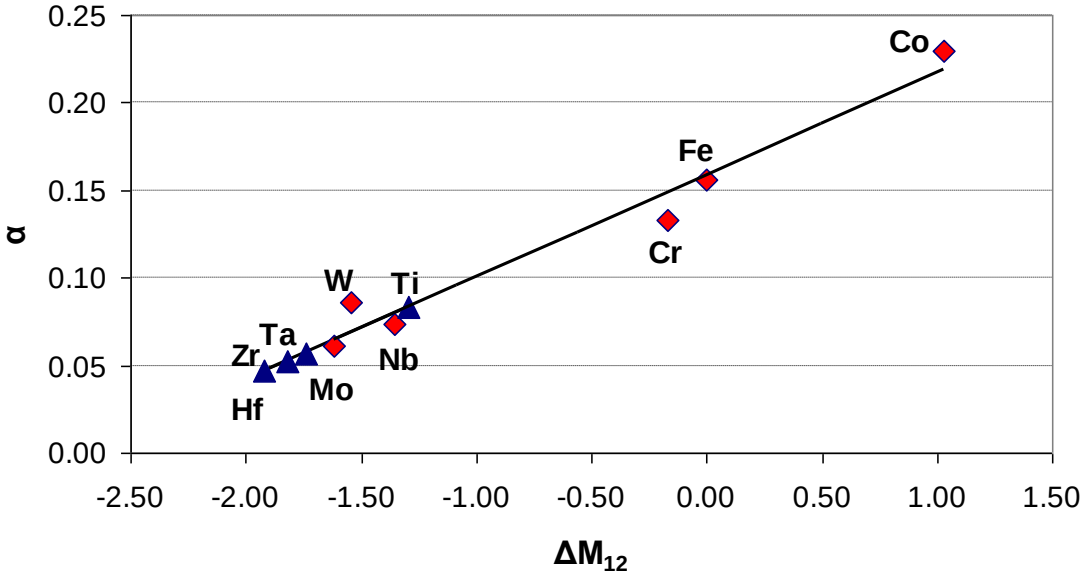

Extension of Diffusion Modeling

- Complete systematic calculations of impurity diffusivities for 3d, 4d, and 5d solutes
  - Initial tests underway to increase efficiency of calculations
  - Develop further the model for magnetic effects on activation energies in paramagnetic state using special quasirandom supercell structures to model magnetic disorder

- Extend calculations to concentrated mixtures
  - Compute vacancy-hopping frequencies as a function of chemical environment employing approaches described in previous slides
  - Use results to build up a kinetic-Monte-Carlo simulation for binary systems
  - Compute diffusion coefficients as a function of temperature and concentration from analysis of statistics of random walks for individual atoms (self or tracer diffusion) or for center of mass of atomic positions (interdiffusion)

Parameters for Dislocation Dynamics Models

- Parameters for solid-solution strengthening
  - Misfit parameters and composition-dependent elastic constants for elastically mediated solute-dislocation interactions
- Parameters for dislocation-precipitate interactions
  - Composition dependent stacking-fault and antiphase-boundary energies for ordered intermetallic phases, important for processes involving shearing of dislocations
  - Composition-dependent lattice parameters and elastic moduli for elastically-mediated interactions

National Center for Electron Microscopy

High resolution TEM micrograph of a single $Al_3(Li,Sc)$ core-shell precipitate in Al

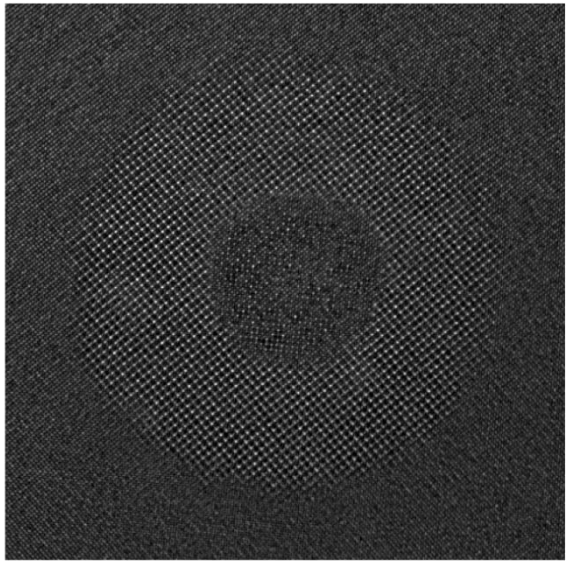

HAADF image of core-shell interface; arrows show alignment of the (Sc,Li) sublattice with the Li sublattice

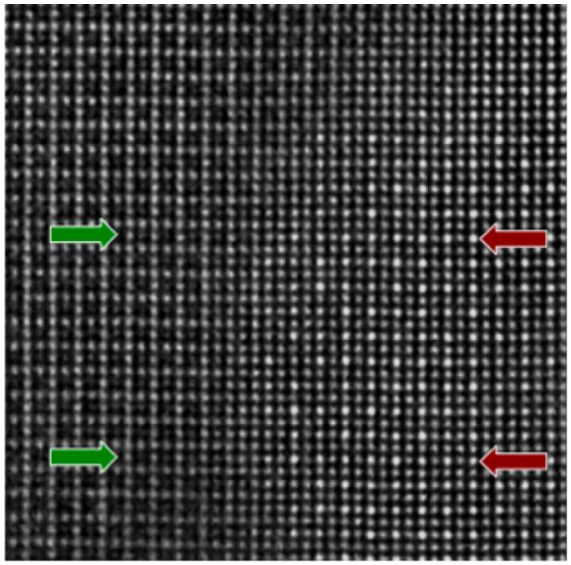

Pairwise interaction energies between Li and Sc atoms in an Al matrix showing binding at 2nd and 4th neighbor shells

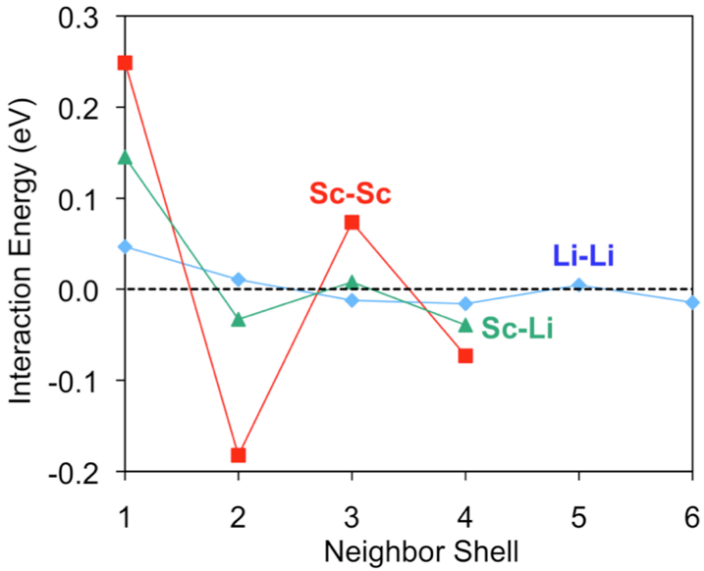

V. Radmilovic, C. Ophus, E. A. Marquis, M. D. Rossell, A. Tolley, A. Gautam, M. Asta and U. Dahmen, *Nature Mat.* (to be submitted).

Prof. Dunand's Presentation
Previous Results

Project Objectives

- Task 5: Creep Behavior
  1. Creep experiments
  2. Neutron-diffraction study
  3. Dislocation-dynamics simulations

NiAl-type precipitates in Fe matrix

TEM BF showing coherency strain contrast

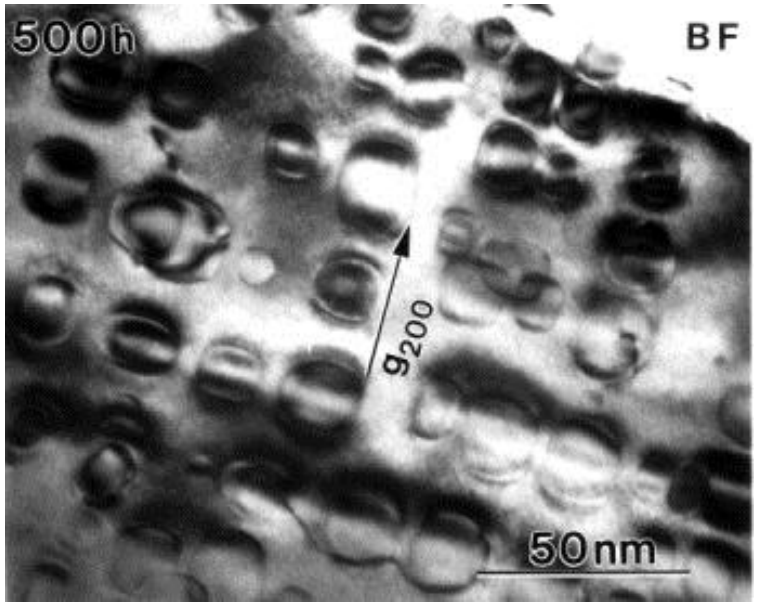

TEM DF (using 100-type reflections) showing B2 precipitates

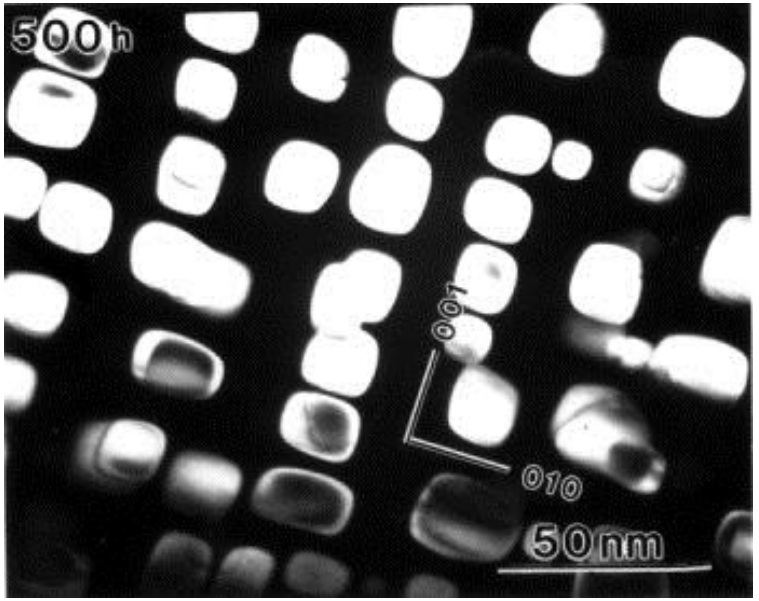

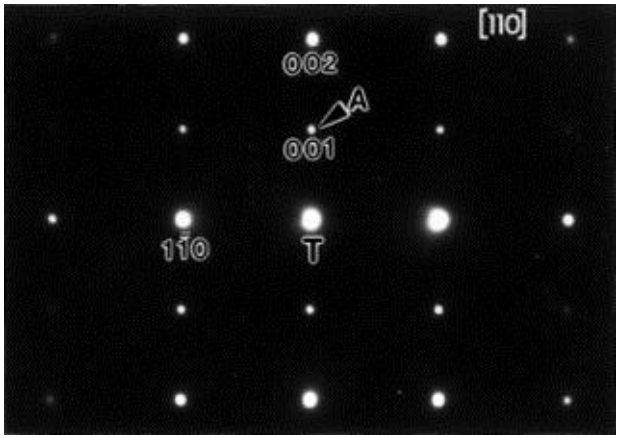

G. Ghosh, Unpublished research, NU

Ni_2Ti Al-Heusler precipitates in an Fe matrix

TEM DF (using 100-type reflections)
Common to both *B*2 and $L_2$1 structures

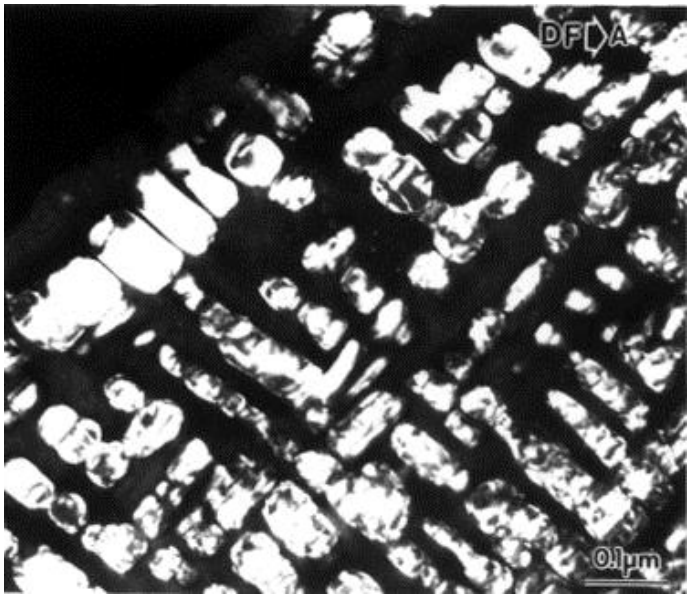

TEM DP showing reflections of both
*B*2 and $L_2$1 type structures

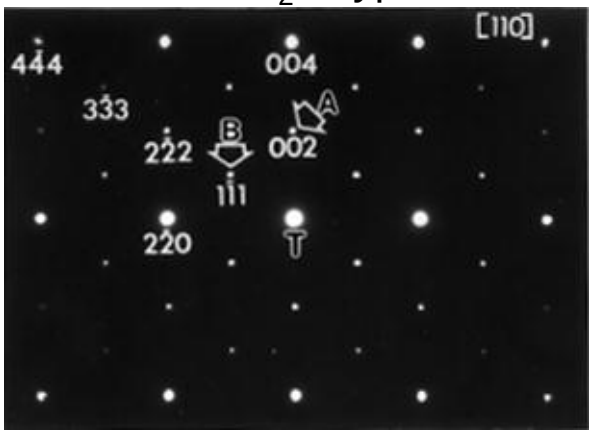

TEM DF (using 111-type reflections)
Unique to $L_2$1 structures

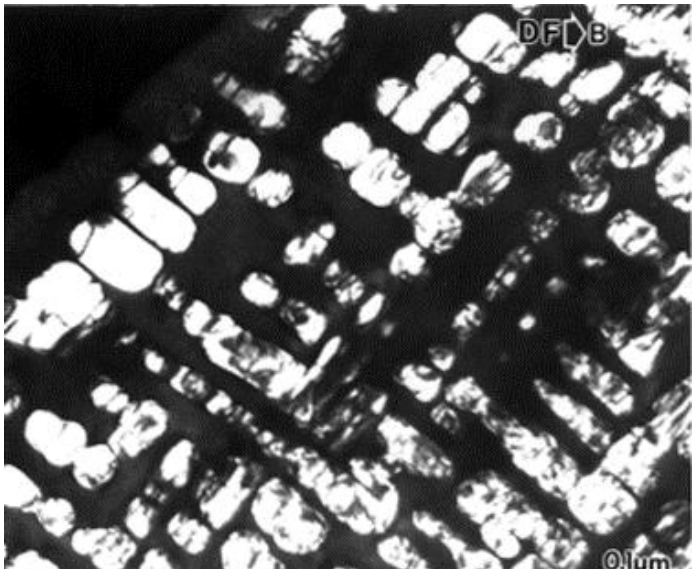

G. Ghosh, Unpublished research, NU

Hierarchical microstructure: NiAl-type + Ni_2TiAl-type precipitates

TEM BF micrograph

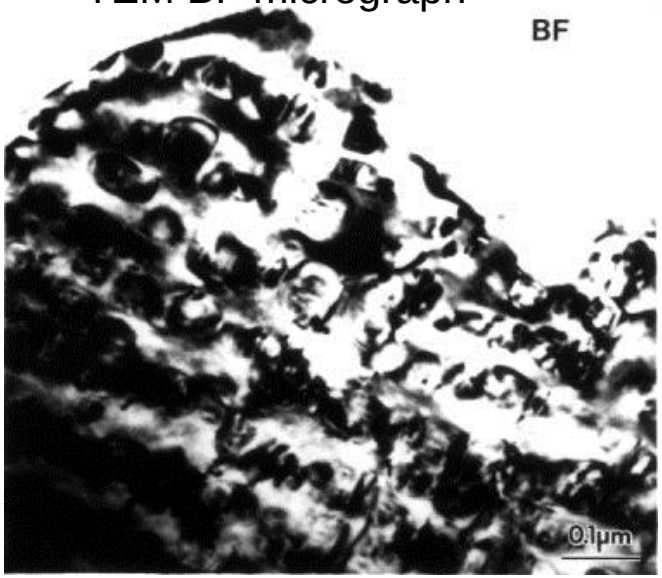

TEM DP showing reflections of both *B*2 and $L_2$1 type structures

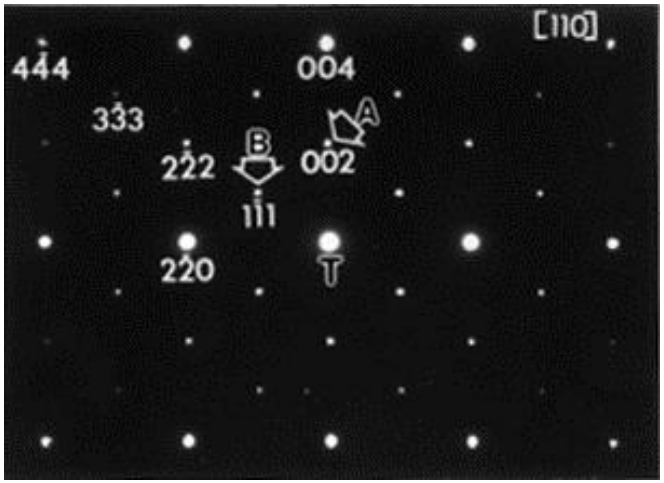

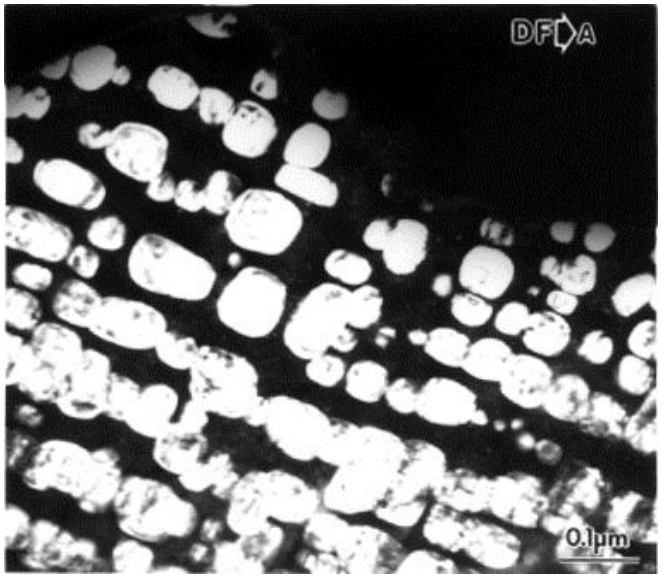

TEM DF using (200)-type *B*2/$L_2$1 spots

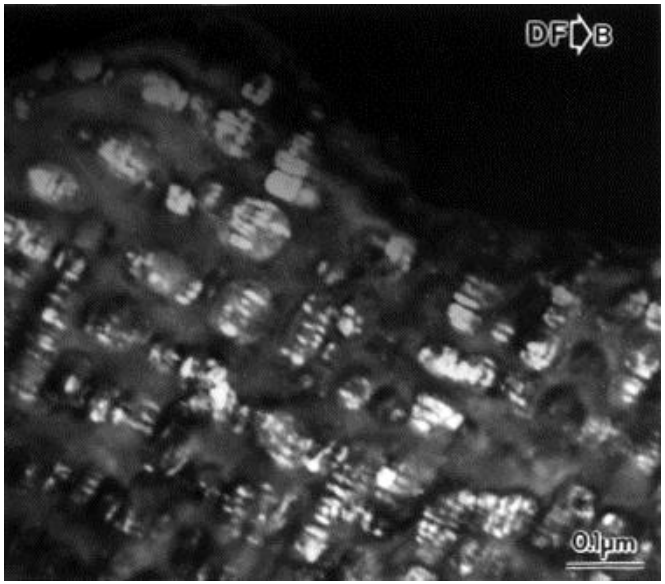

TEM DF using (111)-type $L2_1$ spots (unique)

G. Ghosh, Unpublished research, NU

Alloy Development

Alloys #	Fe (wt. %)	Al	Cr	Ni	Mo	Zr	B
FBB10	66.3	10	10	10	3.4	0.25	0.005
FBB8	68.3	8	10	10	3.4	0.25	0.005
FBB6.5	69.8	6.5	10	10	3.4	0.25	0.005
FBB6	70.3	6	10	10	3.4	0.25	0.005
FBB5	71.3	5	10	10	3.4	0.25	0.005
FBB4	72.3	4	10	10	3.4	0.25	0.005

Parameters Alloys		Average diameter	Average spacing
FBB4	Aged	152.4 ± 6.2	302.0 ± 11.5
	Crept	159.2 ± 2.8	333.1 ± 7.9
FBB5	Aged	127.4 ± 3.8	229.5 ± 14.0
	Crept	117.4 ± 3.8	240.4 ± 2.6
FBB6	Aged	111.0 ± 3.0	186.6 ± 3.2
	Crept	119.4 ± 3.0	183.9 ± 3.1
FBB6.5	Aged	129.8 ± 4.2	175.0 ± 4.9
	Crept	119.0 ± 1.7	210.9 ± 1.4
FBB8	Aged	99.4 ± 1.5	178.5 ± 1.5
	Crept	109.4 ± 1.8	196.9 ± 2.2
FBB10	Aged	89.6 ± 2.0	180.1 ± 1.6

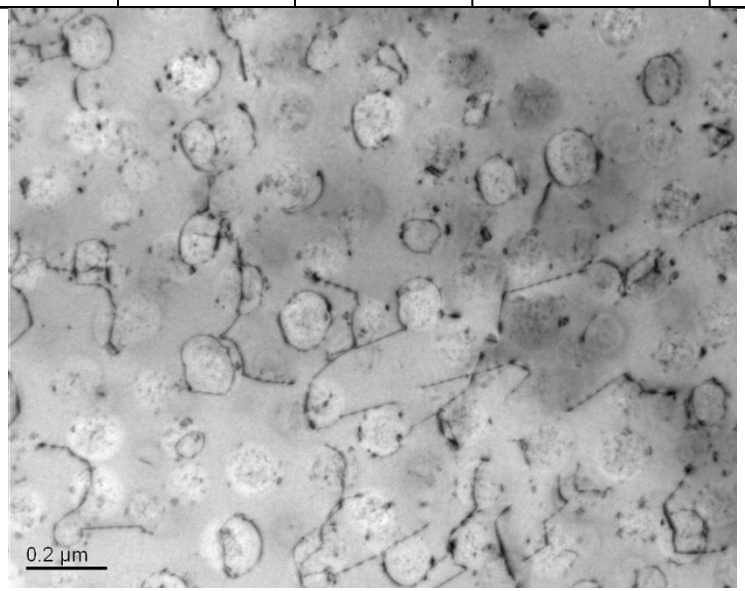

Effects of Al on the Creep Behavior and Microstructures in a (Ni,Fe)Al Precipitate-Strengthened Ferritic Superalloy
S Huang, X Li, G Ghosh, E Kenik, J Ilavsky, Z Teng, G Wang, ME Fine, CT Liu, L Liu, PK Liaw (in preparation)

Creep Behavior at 700 ºC

Compression

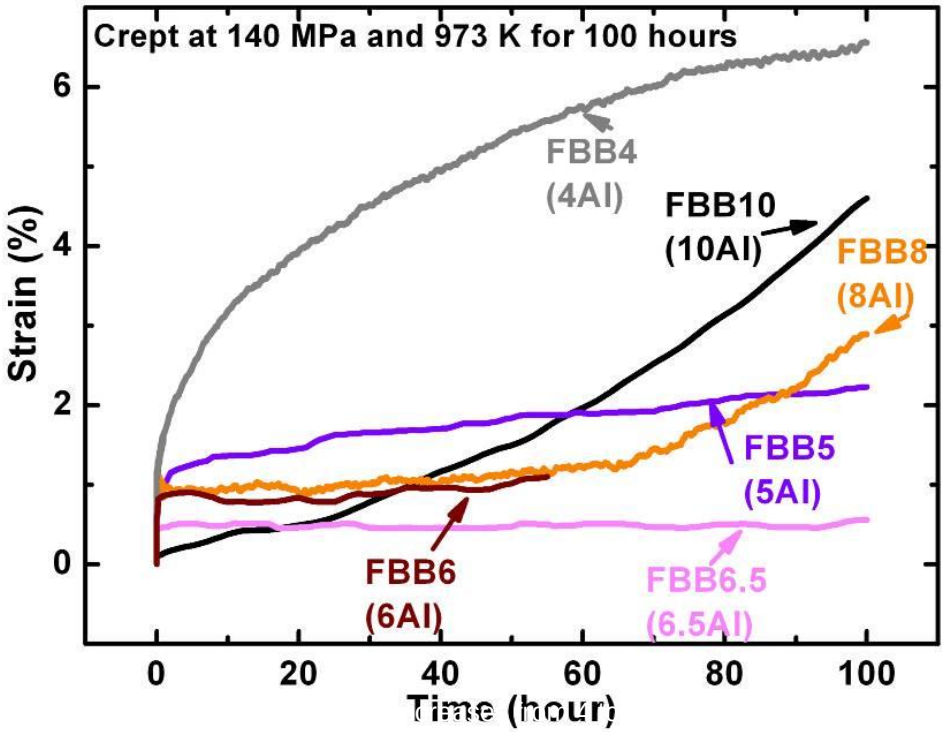

Tension (FBB6.5)

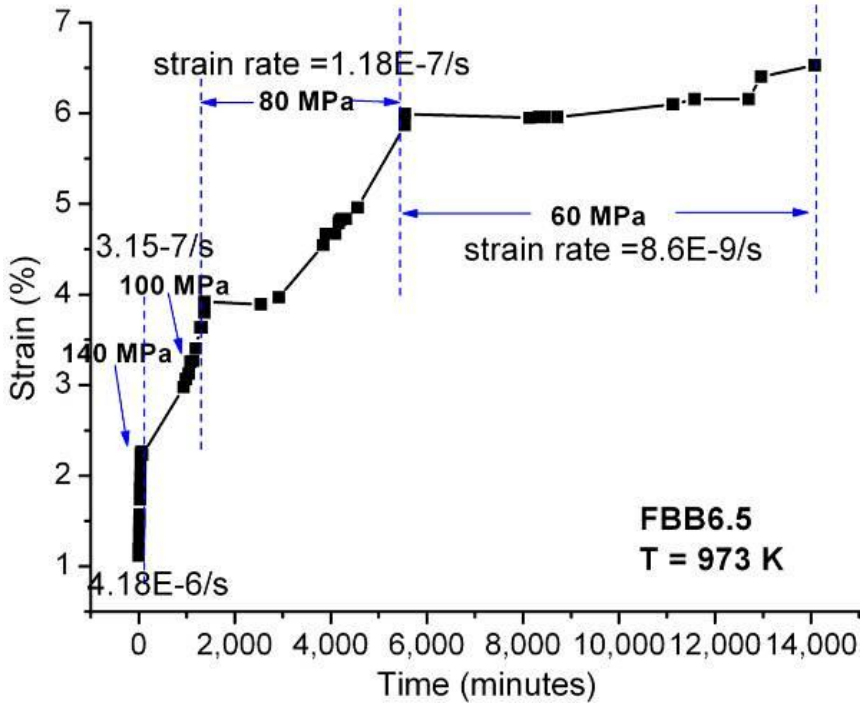

Effects of Al on the Creep Behavior and Microstructures in a (Ni,Fe)Al Precipitate-Strengthened Ferritic Superalloy
S Huang, X Li, G Ghosh, E Kenik, J Ilavsky, Z Teng, G Wang, ME Fine, CT Liu, L Liu, PK Liaw (in preparation)

Crept Microstructure

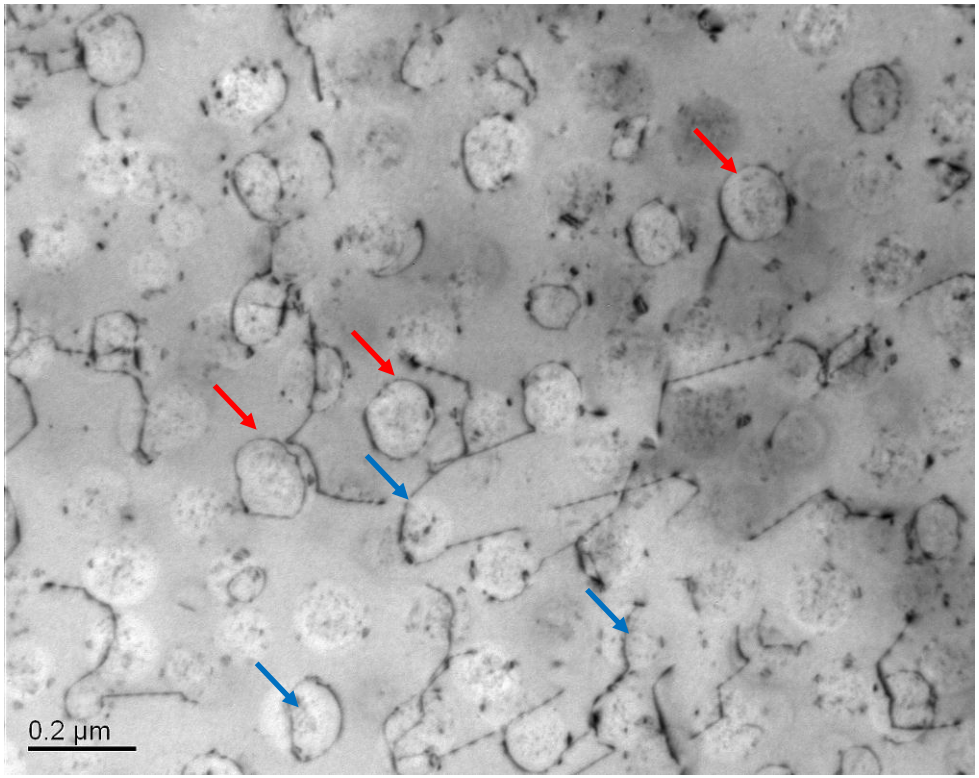

Bright-field images of compressively crept FBB8 alloy (110 diffraction vector near [001] zone)

1. dislocation loop around particles – Orowan mechanism (red arrows)
2. dislocation climb above particles (blue arrows).

Effects of Al on the Creep Behavior and Microstructures in a (Ni,Fe)Al Precipitate-Strengthened Ferritic Superalloy
S Huang, X Li, G Ghosh, E Kenik, J Ilavsky, Z Teng, G Wang, ME Fine, CT Liu, L Liu, PK Liaw (in preparation)

1. Creep Experiments

1. Extend measurements for FBB6 (10^{-4} – 10^{-9} s^{-1})

Compression Creep
- effect of stress 40-200 MPa (stress exponent)
- effect of temperature 600-700 ºC (activation energy)

Tension Creep
- effect of stress 40-200 MPa (stress exponent)
- effect of temperature 600-700 ºC (activation energy)
- measure primary creep
- measure tensile ductility + fracture time

Model Creep
- Simple creep equations
- Dislocation dynamics
- -> predict optimal microstructure

$$\dot{\varepsilon} = A\sigma^n \exp\left(-\frac{Q}{RT}\right)$$

$$t_f\dot{\varepsilon} = C$$

$$\frac{t_f\dot{\varepsilon}}{\varepsilon_f} = C'$$

Microstructure before and after creep
- Grain size
- Precipitate size and spacing
- Ambient tensile properties

2. Perform above measurements on new alloys

2. Neutron diffraction during creep (with UT team)

For optimal creep conditions (~100 MPa, 700ºC), determine elastic strains by diffraction in both phases

Determine strain and stress partitioning to particle

Finite Element modeling

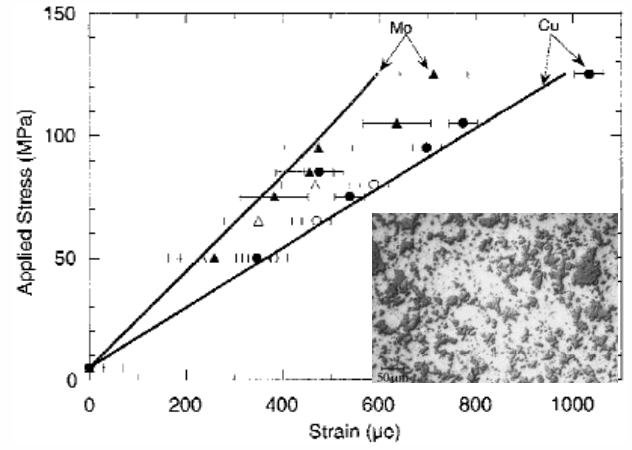

Cu-15Mo

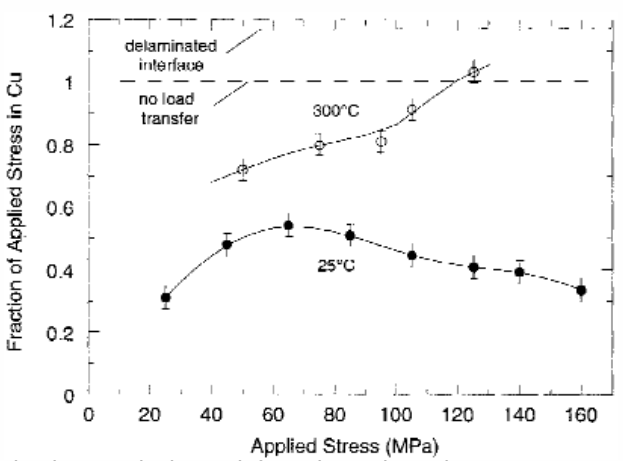

M.R. Daymond, C. Lund, M.A.M. Bourke, D.C. Dunand, "Elastic phase-strain distribution in a particulate-reinforced metal-matrix composite deforming by slip or creep", *Metallurgical and Materials Transactions*, **30A**, 11A, 2989-2997 (1999).

3. Dislocation Dynamics Modeling

Dislocation Models – Closed Form Solutions

1. Precipitate Shearing
   a. Elastic interactions:
      i. Lattice parameter misfit (δ)
      ii. Shear modulus mismatch (Δμ)
   b. Order (γ_{APB})

2. Orowan looping (bypass)

1ai. and 1aii. : ***additive***

1a. and 1b. : ***series*** (larger prevails)

1. and 2. : ***parallel*** (smaller prevails)

$$\Delta\tau_{coh} = \alpha_{\varepsilon}\left(\mu|\varepsilon|\right)^{3/2}\sqrt{\frac{\langle r\rangle\phi}{\mu b/2}}$$

$$\Delta\tau_{\mathrm{mod}} = 0.0055\,\Delta\mu^{3/2}\sqrt{\frac{2\phi}{\mu}}\left(\frac{\langle r\rangle}{b}\right)^{(3m-2)/2}$$

$$\Delta\tau_{ord} = 0.81\frac{\gamma_{APB}}{2b}\sqrt{\frac{3\pi\phi}{8}}$$

$$\Delta\tau_{Or} = \frac{0.4\,\mu b}{\pi\sqrt{1-\upsilon}}\left[\frac{\ln\left(2\bar{r}/b\right)}{\langle r\rangle\left(\frac{1.538}{\sqrt{\phi}}-1.643\right)}\right]$$

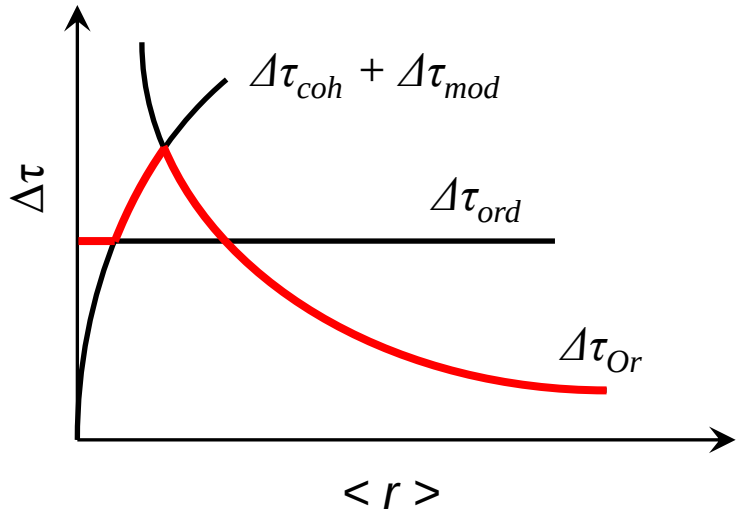

Modeling of complex precipitates

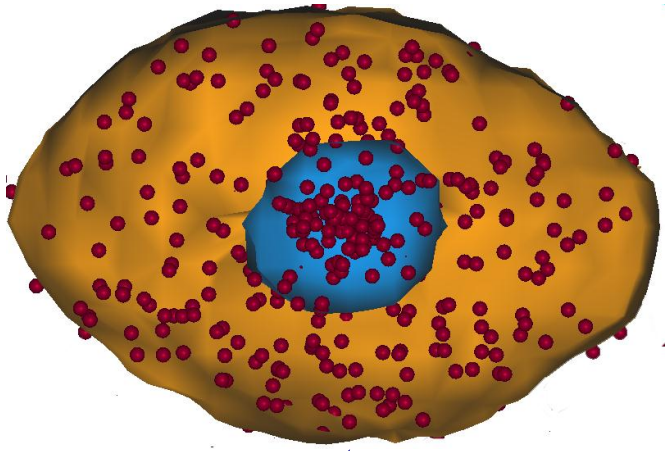

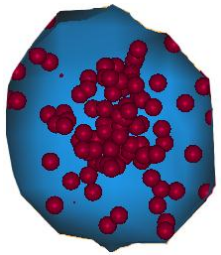

M.E. Krug, D.C. Dunand, D.N. Seidman
"Effects of Li Additions on Precipitation-Strengthening Al-Sc and Al-Sc-Yb Alloys"
Acta Materialia, 59, 1700-1715 (2011)

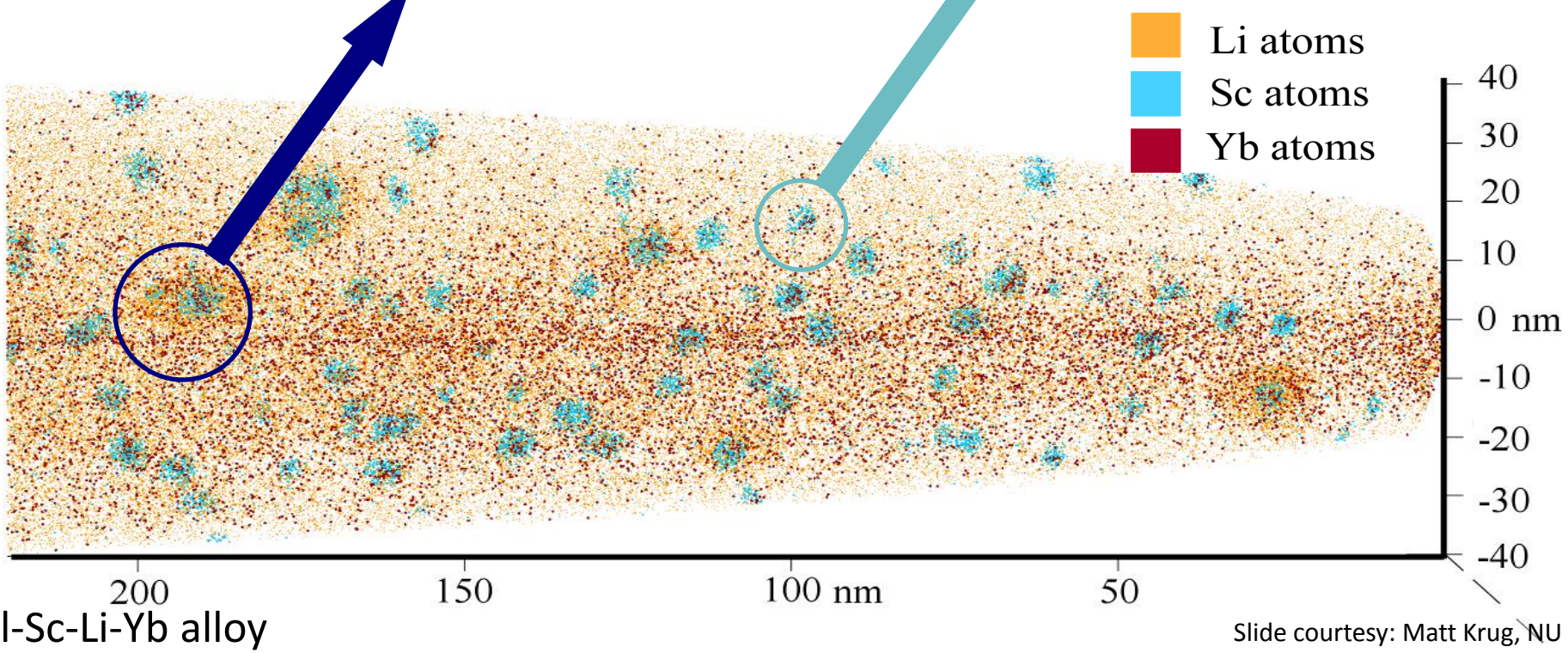

Al-Sc-Li-Yb alloy

Slide courtesy: Matt Krug, NU

Our Precipitate Structure

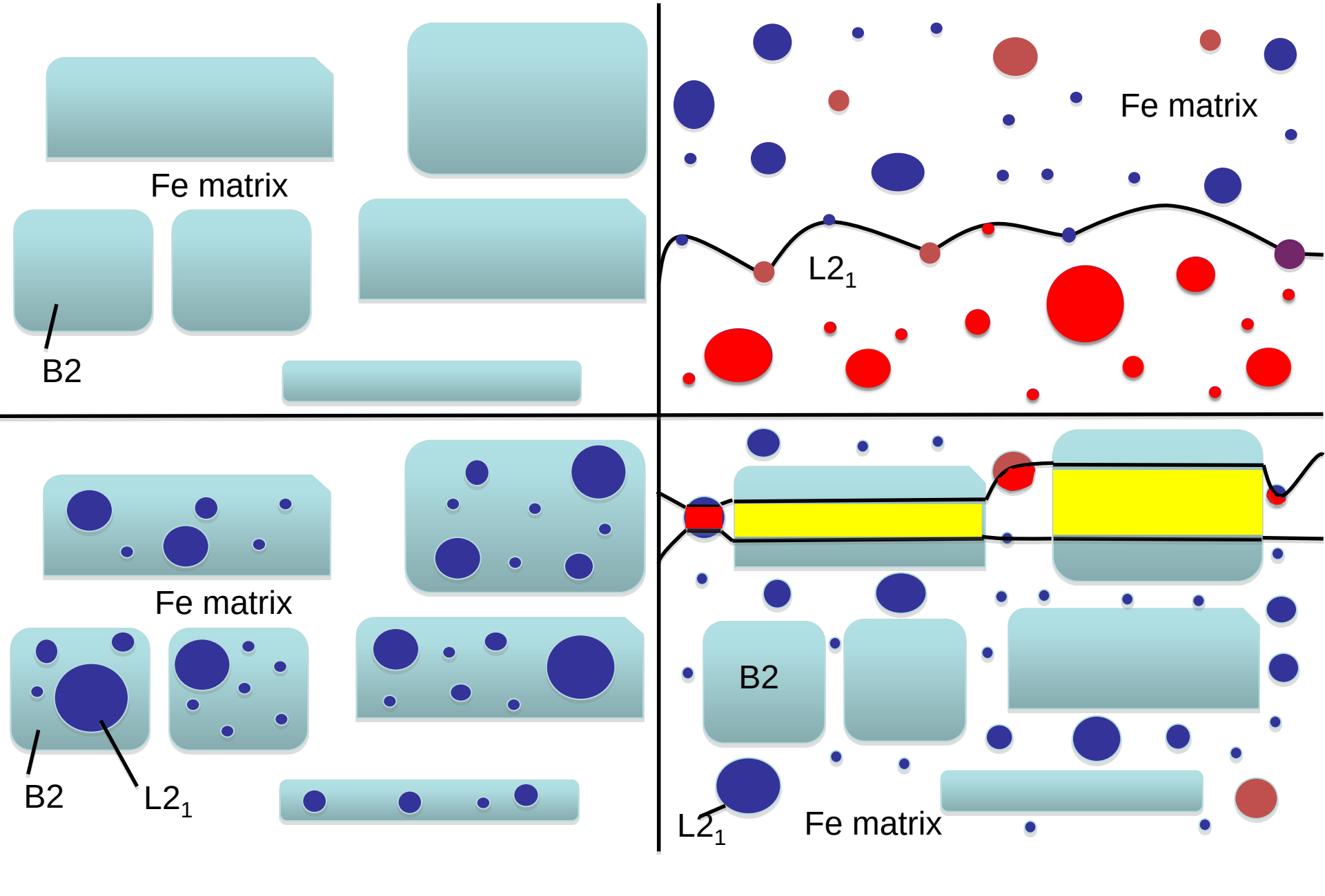

Dislocation-Dynamics Modeling: Method

Mohles V. Phil. Mag. A 2001;81:971

$$\tau_{ext} = -\left(\tau_{disloc} + \tau_{drag} + \tau_{obst}\right)$$

imposed, incremented throughout simulation

dislocation self-interaction stress

internal friction of the lattice

interaction stress between dislocation and precipitate

τ_{obst} : γ_{APB}

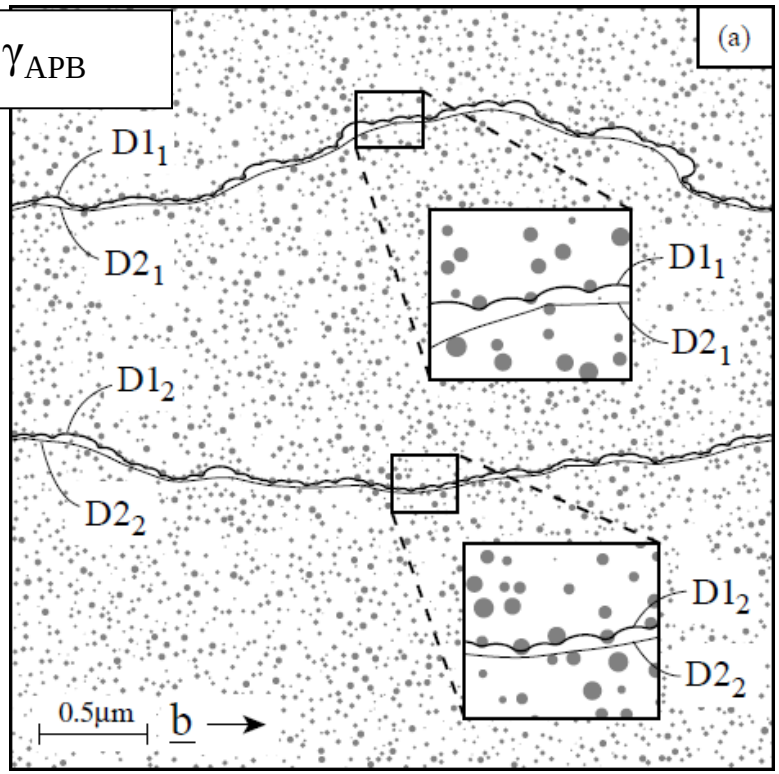

Mohles V. Mater. Sci. Eng. A 2004;365:144.

τ_{obst} : $\delta_{matrix/precip.}$

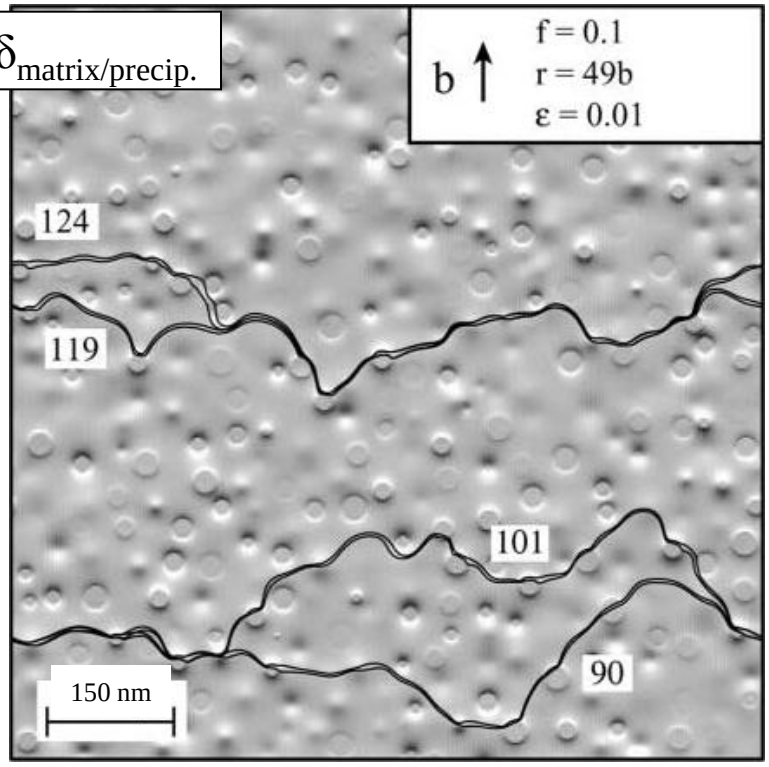

Mohles V, Nembach E. Acta Mater. 2001;49:2405.

Slide courtesy: Matt Krug, NU

Dislocation-Dynamics Modeling: Capturing the Dataset

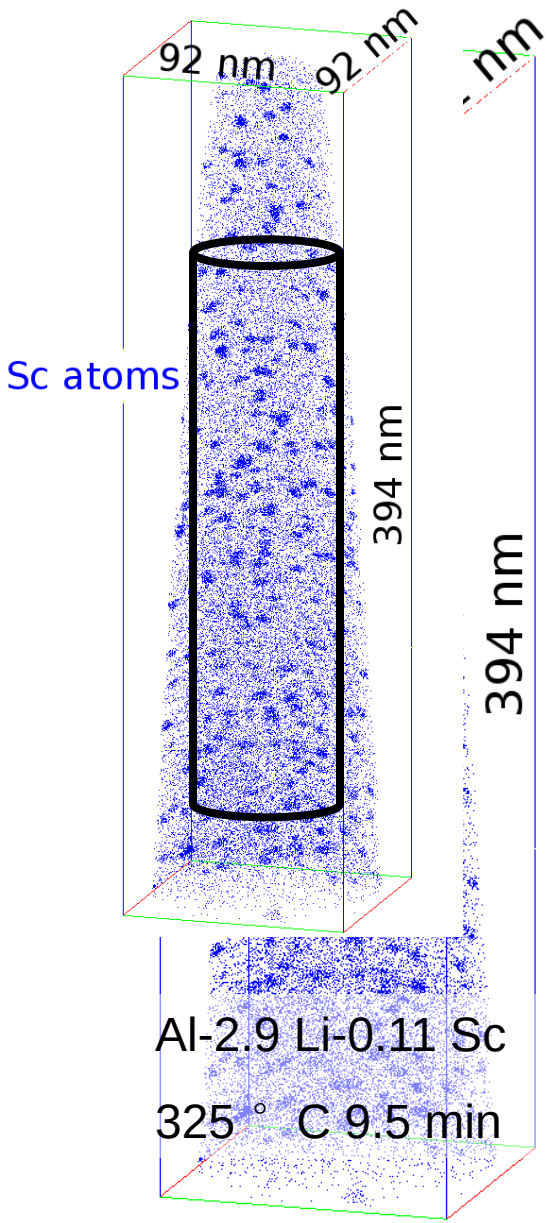

1. Isolate precipitates- cluster search algorithm:

   Each precipitate i : (x_i y_i z_i r_i)

- Find largest inscribed cylinder
- Apply random symmetry operations:

  rotations, mirrors, translations
- Assemble resulting cylinders
- Cut through common plane to create glide plane

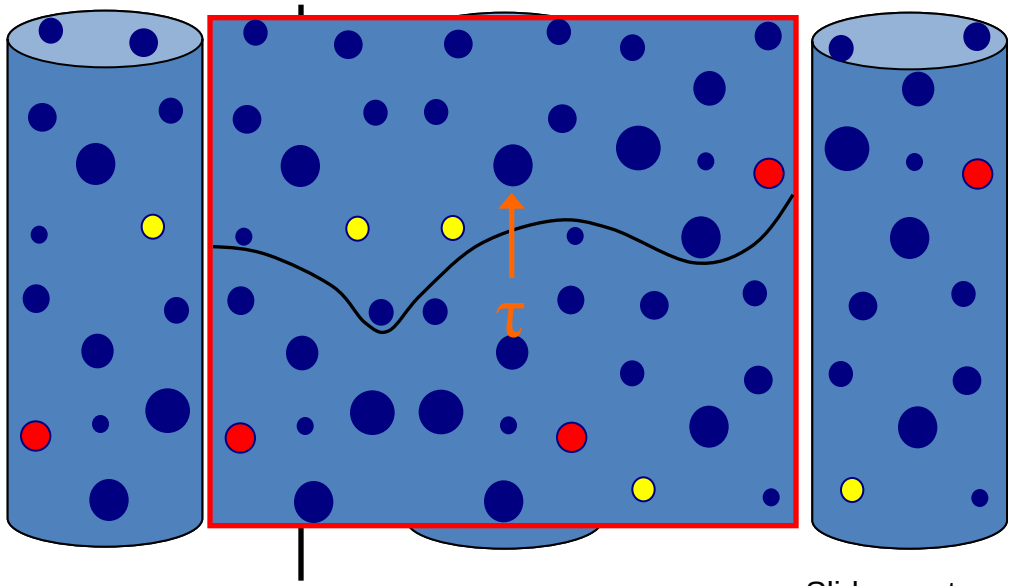

Slide courtesy: Matt Krug, NU

Dislocation-Dynamics Modeling: Example APT Dataset

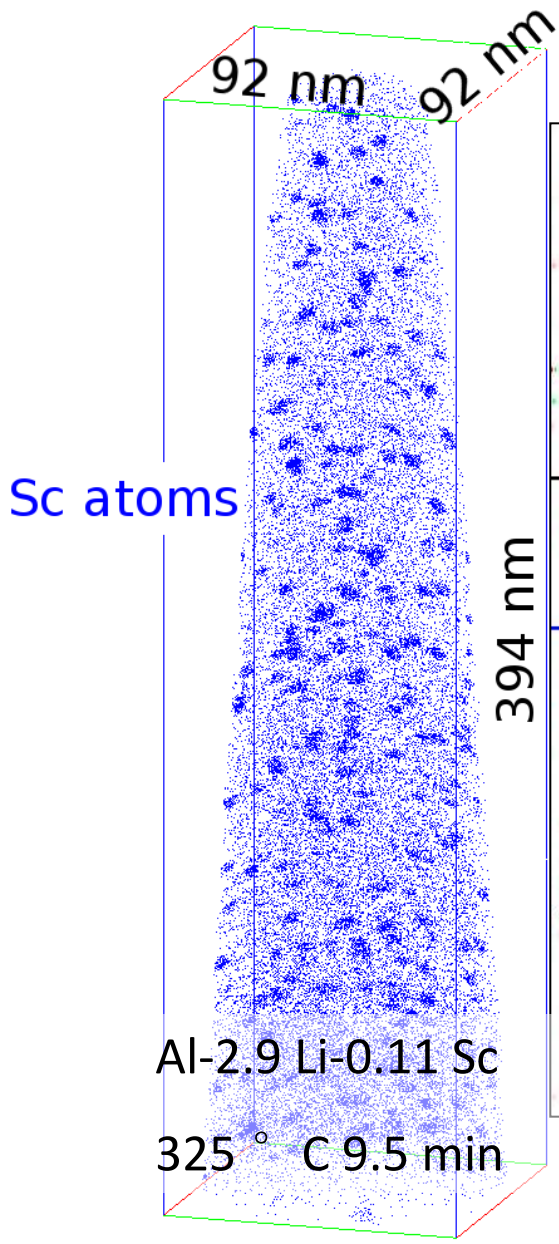

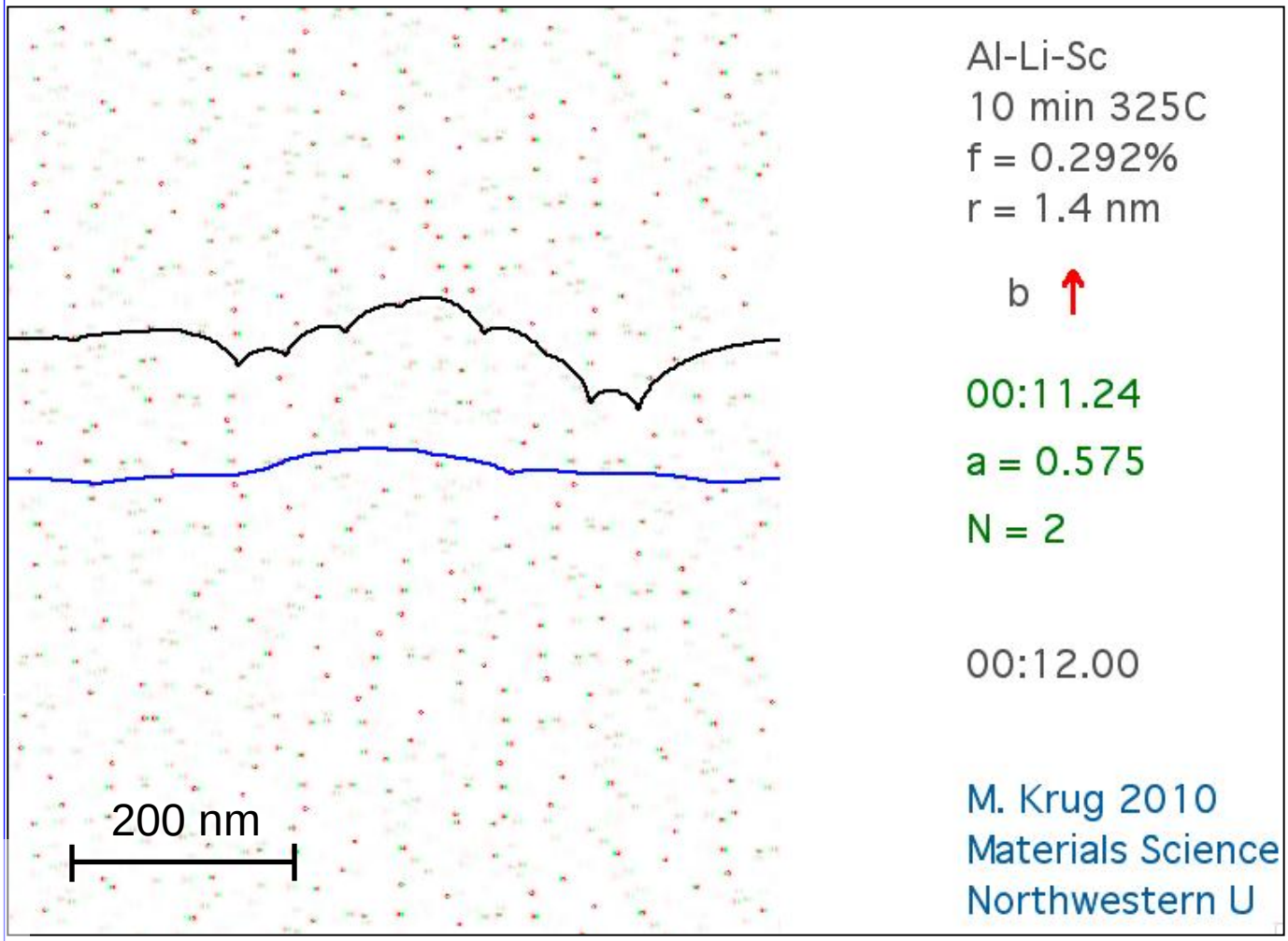

Dislocation-Dynamics Modeling: Example APT Dataset

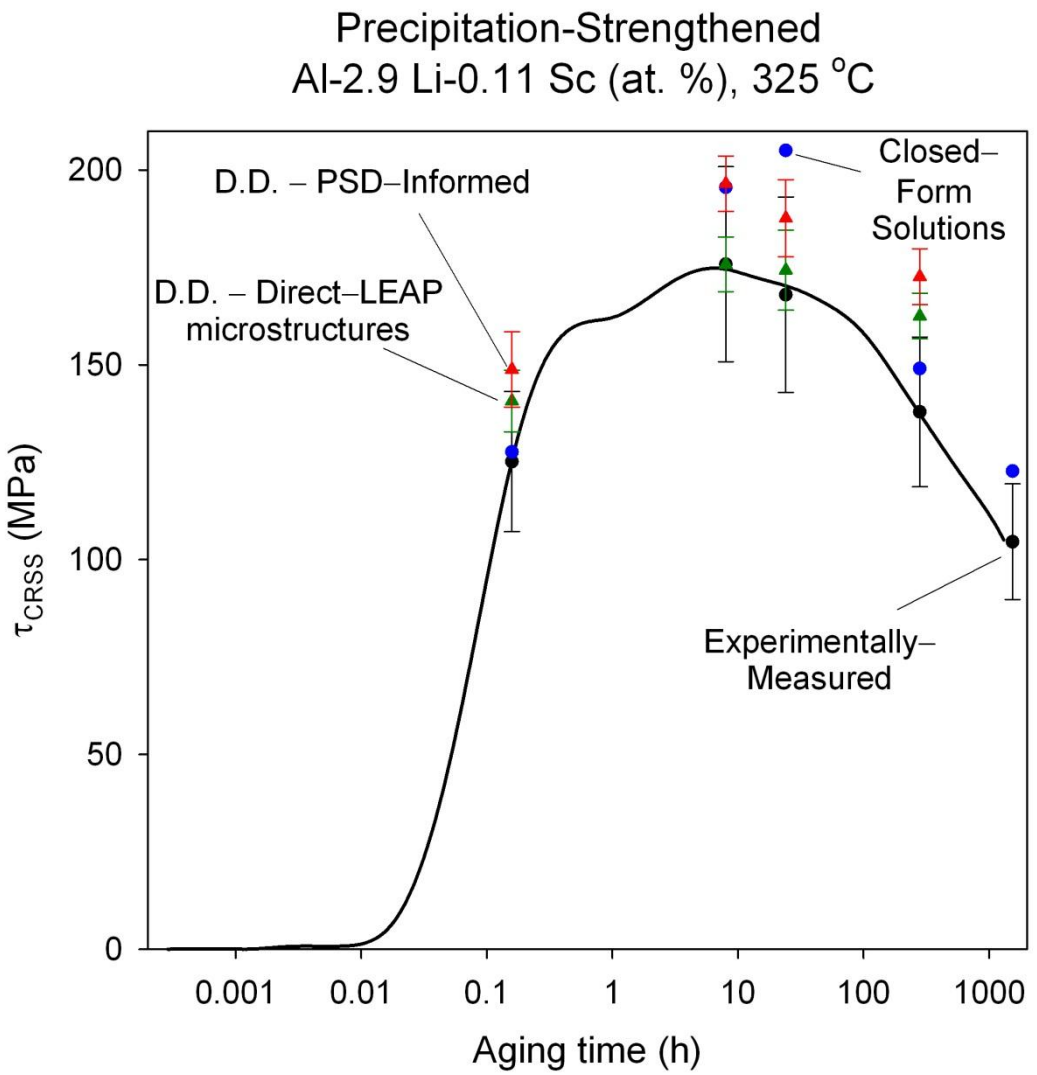

- Closed-Form solutions do well for under- and over-aged, overshoot and miss peak strength
- PSD-informed: overshoots consistently
- Direct LEAP microstructures: captures underaged and peak, overshoots overaged strength.

Slide courtesy: Matt Krug, NU

Dislocation Dynamics Modeling: Example Core-shell APT Dataset

Al-Li-Sc alloy

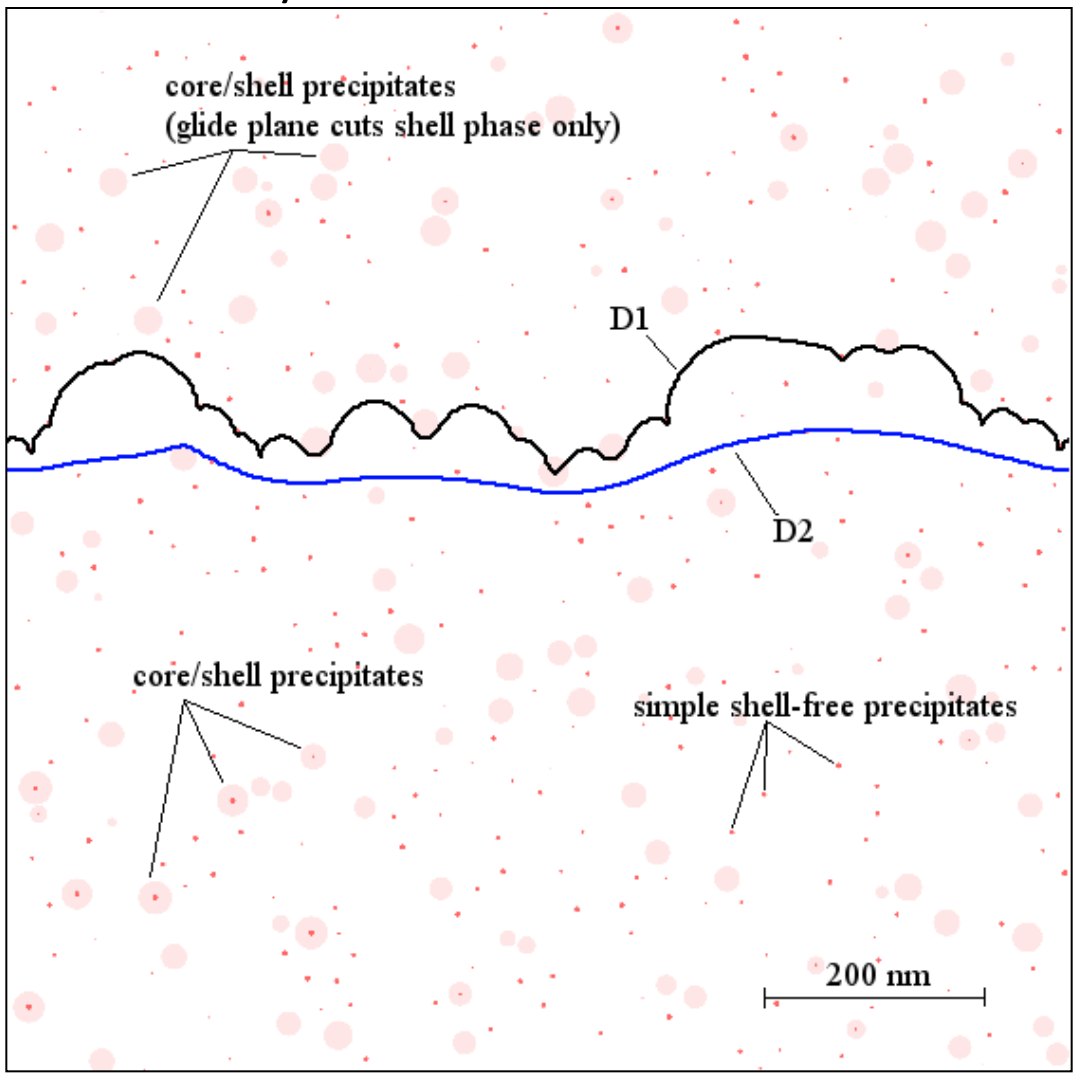

Core-shell precipitates: successfully demonstrated

Adapt to steel alloys

- Higher volume fraction
- Different geometry
- Various Radii
- Exploring parameter space
- Designing optimum heat treatment

Slide courtesy: Matt Krug, NU

Strength Modeling

- LEAP-measured datasets simulated
- Model extended to allow:
  1. Modulus strengthening
  2. Multiple strengthening mechanisms simultaneously
  3. Core/shell precipitate structures
- Preliminary results are encouraging for the Al-Li-Sc
- Expand the model to complex steel microstructures

Prof. Liaw's Presentation
Previous Results

Schematic Diagram of LEAP

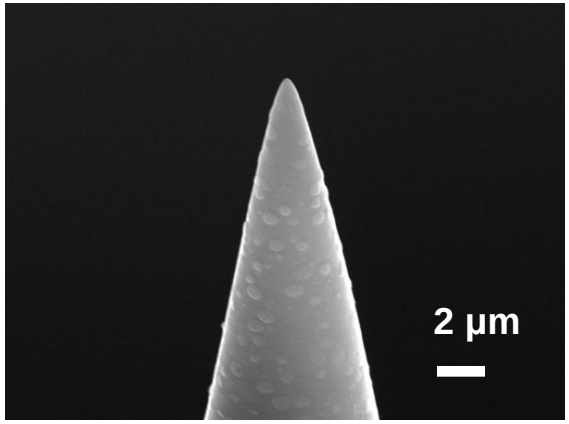

Oak Ridge National Laboratory

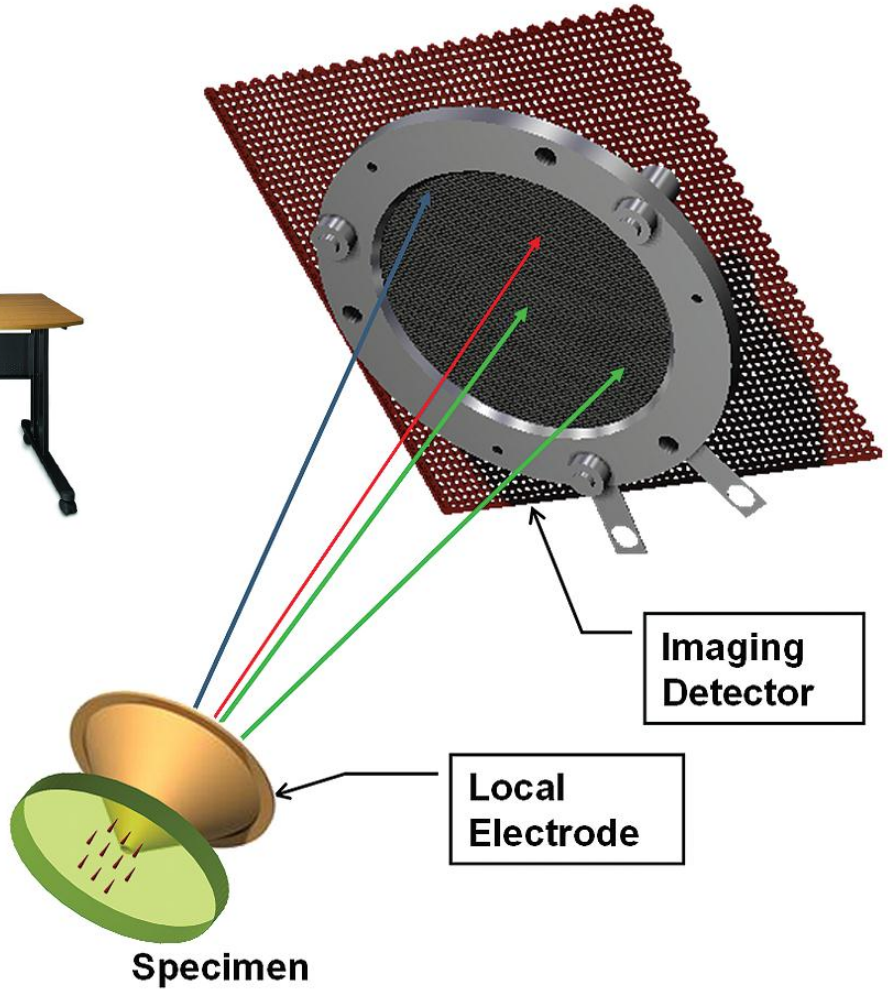

D. J. Larson and T. F. Kelly, Imago Scientific Instruments Corporation, Madison, WI, USA

Atom Probe Tomography Characterizations

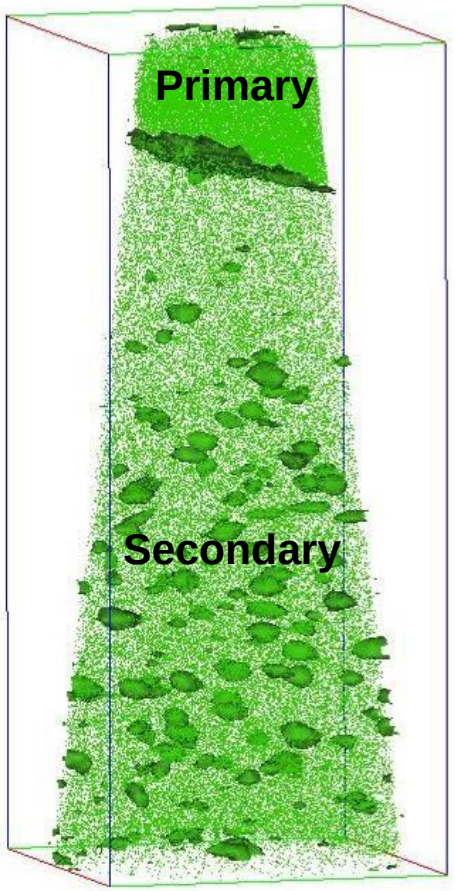

15 at.% Al iso-concentration surface

10 nm

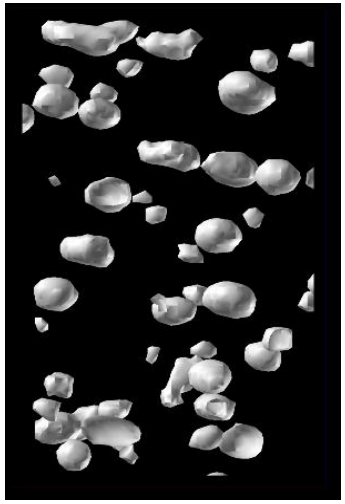

Morphology of secondary precipitates

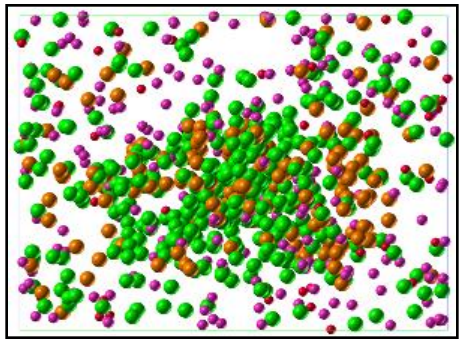

2 nm

Atom map of a selected secondary precipitate

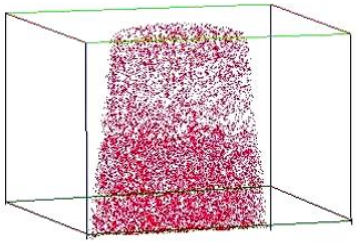

Mo atom map

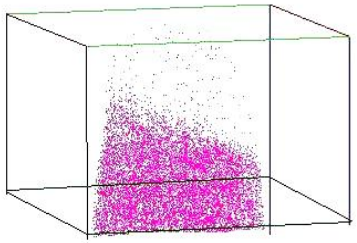

Cr atom map

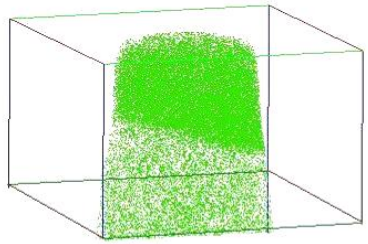

Al atom map

APT revealed a duplex precipitation of NiAl particles: primary with an diameter of 130 nm ($Ni_{41.2}Al_{43.6}Fe_{12.7}Cr_{0.8}Mo_{1.4}$) and secondary with an diameter of 3 nm ($Ni_{26.3}Al_{41.6}Fe_{26.9}Cr_{3.3}Mo_{1.7}$).

Z.K. Teng, M.K. Miller, G. Ghosh, C.T. Liu, S. Huang, K.F. Russell, M.F. Fine, and P.K .Liaw. Scripta Mater. 63, 61 (2010).

Concentration Profiles

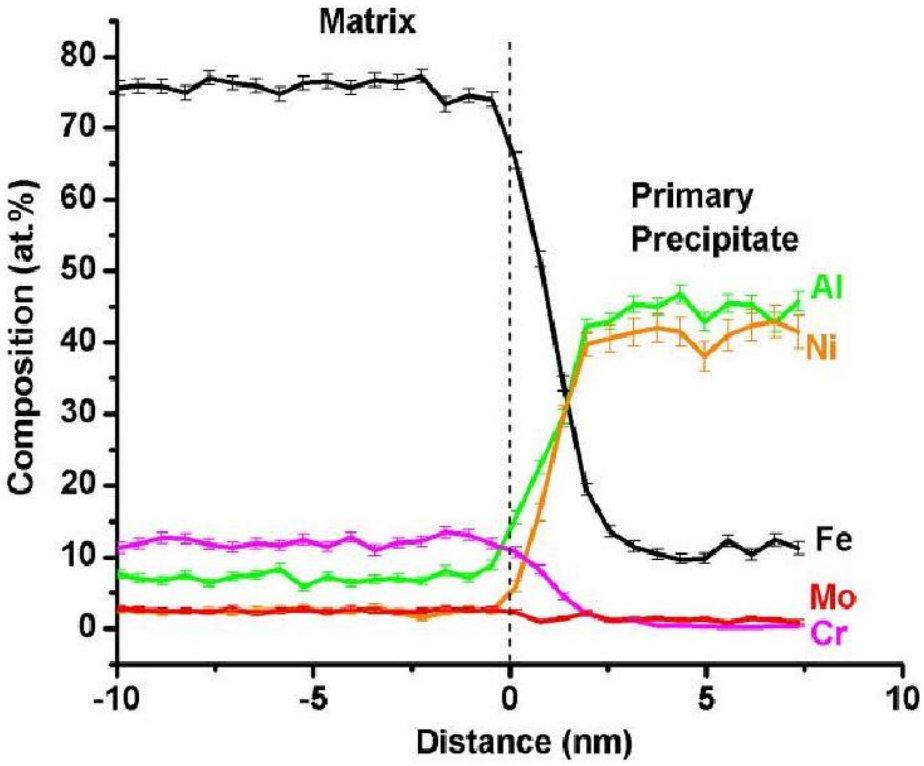

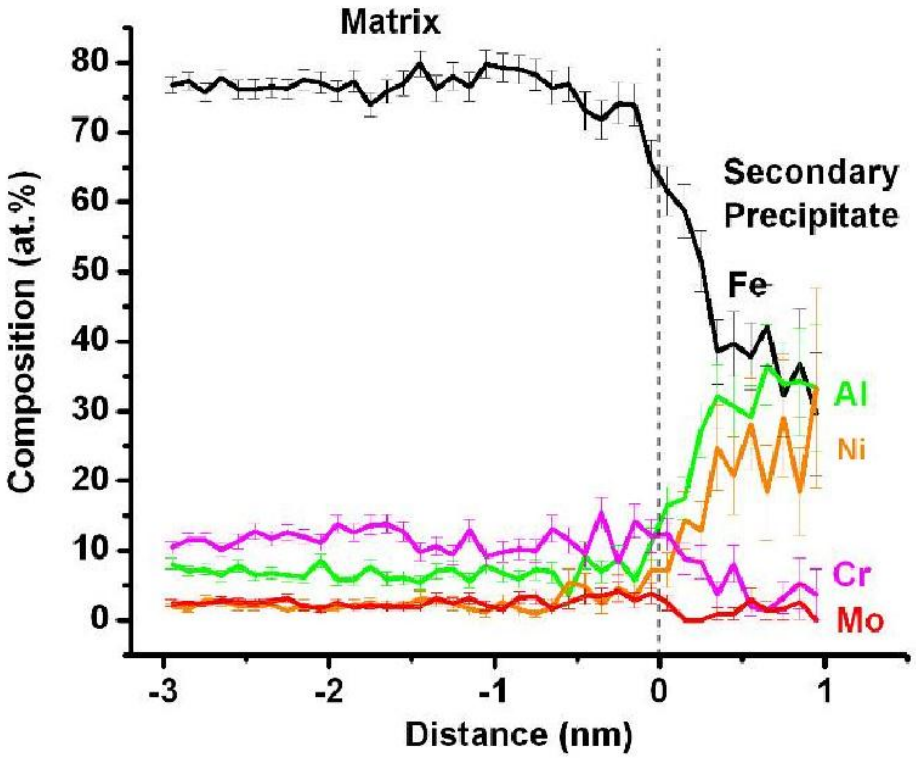

APT revealed a duplex precipitation of NiAl particles: primary with an diameter of 130 nm ($Ni_{41.2}Al_{43.6}Fe_{12.7}Cr_{0.8}Mo_{1.4}$) and secondary with an diameter of 3 nm ($Ni_{26.3}Al_{41.6}Fe_{26.9}Cr_{3.3}Mo_{1.7}$).

Z.K. Teng, M.K. Miller, G. Ghosh, C.T. Liu, S. Huang, K.F. Russell, M.F. Fine, and P.K .Liaw. Scripta Mater. 63, 61(2010).

Experimental Setup of USAXS

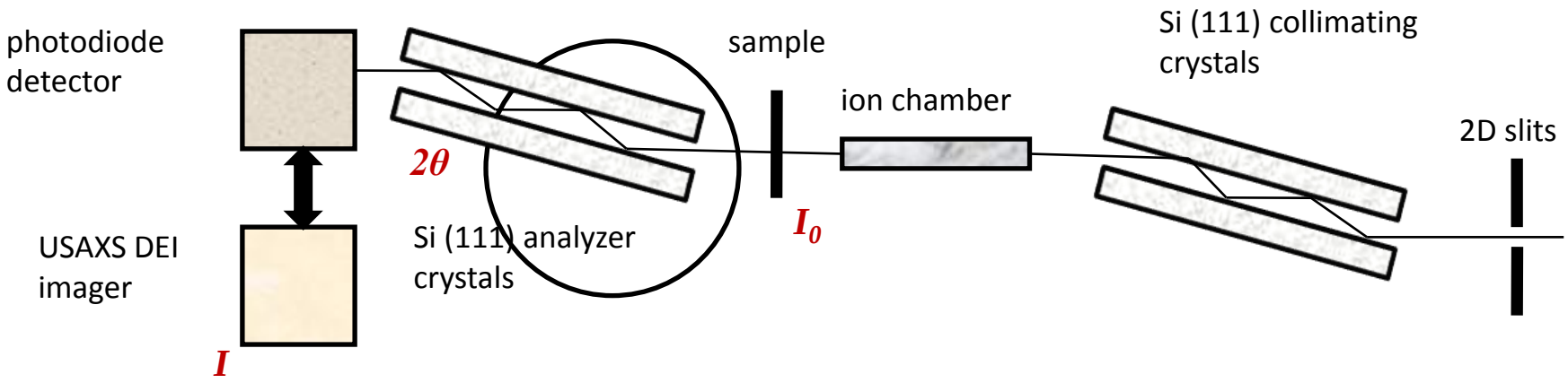

1-D collimated USAXS camera at Advanced Photon Source 15-ID-D, Argonne National Laboratory

Experiment:

- Measured Q range: 10^{-4} ~ 0.5 $Å^{-1}$
- Beam energy: ~ 17 keV
- Beam size: 1.6 x 0.8 mm
- Foil thickness: ~ 50 µm
- Data reduction and desmearing: Irena Package

Theoretical Model for USAXS Data Analysis

Absolute intensity -- *Fourier transformation of electron density*

Non-dilute precipitation: Polydispersity + Interference

Difference in scattering-length density between two phases

Scattering from grain boundaries

Number density of precipitates

Incoherent scattering intensity (background)

One population of precipitates

$$I(Q) = n_p |\Delta\rho|^2 P(Q) S(Q) + AQ^{-b} + I_{INC}$$

Form factor – particle size and shape

$$P(Q) = \left(\frac{4\pi}{3}\right)^2 \int F^2(Q,x) \times N(x,R,\delta) \times x^6 dx$$

$$F(Q,x) = [\sin(Qx) - Qx\cos(Qx)]/(Qx)^3$$

$$N(x,R,\delta) = \exp\left[-(x-R)^2/2\delta^2\right]/\sqrt{2\pi\delta^2}$$

Structure factor – inter-particle correlation

$$S(Q,L,\sigma) = 2\left\{\frac{1-\exp\left(-\frac{Q^2\sigma^2}{4}\right)\cos(QL)}{1-2\exp\left(-\frac{Q^2\sigma^2}{4}\right)\cos(QL)+\exp\left(-\frac{Q^2\sigma^2}{2}\right)}\right\} - 1$$

Non-linear least square fitting for 8 parameters: $n_p|\Delta\rho|^2$, I_{INC}, A, R, δ, L, σ, b

Quantitative Ultra-Small-Angle X-Ray Scattering Analysis

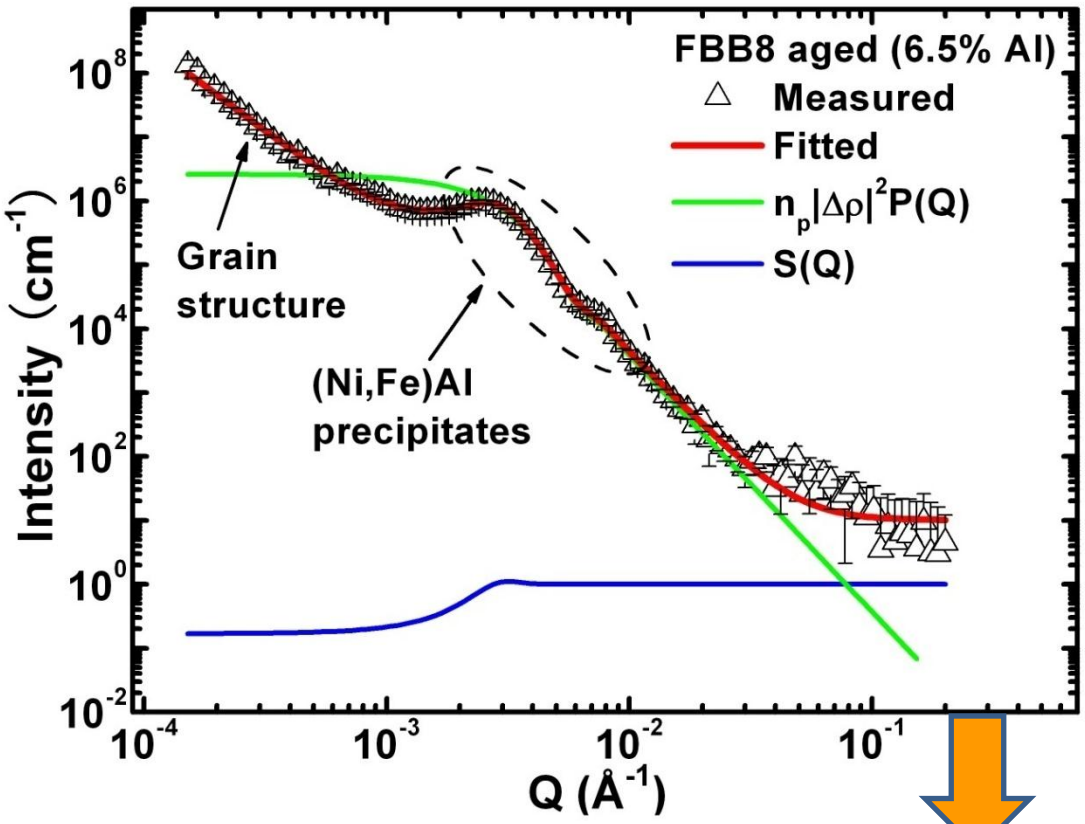

Dark Field Image by 100_{B2} reflection

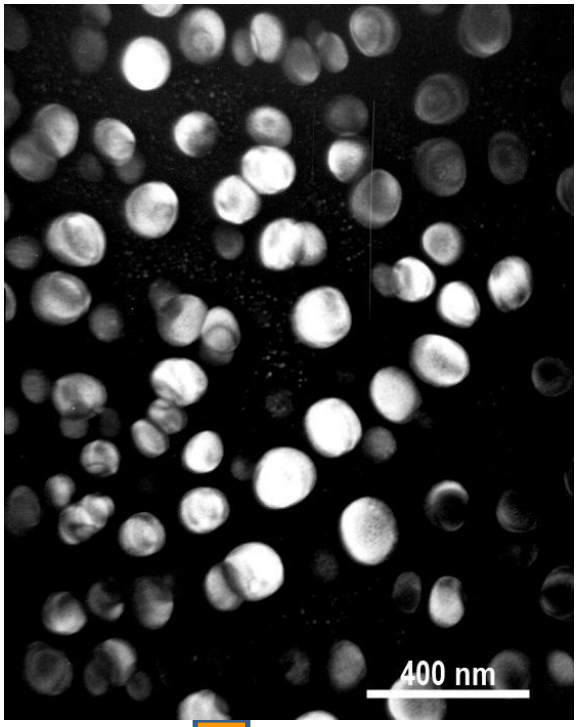

Parameters	USAXS	TEM
Diameter of precipitates	129.8 nm	130 nm
Standard deviation of diameter	30.0 nm	25 nm
Inter-particle spacing	175.0 nm	211 nm
Standard deviation of spacing	101.7 nm	37.5 nm

Proposed Research and Detailed Technical Approach to Achieve the Project Goals

Proposed Microstructural Characterizations (with UC and NU Teams)

- AEM: chemistries of the matrices, precipitates, and the partitioning of alloying elements (e.g., solute partitioning of Ti, Ni, Al, and other elements in ferritic alloys)

- TEM: shape, average size, size distribution, coherency of the B2 and $L2_1$ precipitates, grain/subgrain boundary structures, dislocation-particle, dislocation structures in the crept alloys

- APT: morphology, compositions, and estimated volume fractions of the nano-scaled $L2_1$ and B2 precipitates

- USAXS: precipitate size, size distribution, inter-particle spacing, and volume fraction with the complementary TEM and LEAP characterizations

- XRD: lattice parameters of the matrix and precipitates from ambient to high temperatures, volume fractions of $L2_1$ and B2 phases

Neutron and Synchrotron Facilities (1)

Neutron Sources:

- Spallation Neutron Source, Oak Ridge National Laboratory
- Los Alamos Neutron Science Center , Los Alamos National Laboratory
- ISIS, Rutherford-Appleton Laboratories, United Kingdom
- Australian Nuclear Science and Technology Organization (ANSTO), Australian

Synchrotron Sources:

- Advanced Photon Source, Argonne National Laboratory
- European Synchrotron Radiation Facility (ESRF), France

Neutron and Synchrotron Facilities (2)

Spallation Neutron Source, Oak Ridge National Laboratory

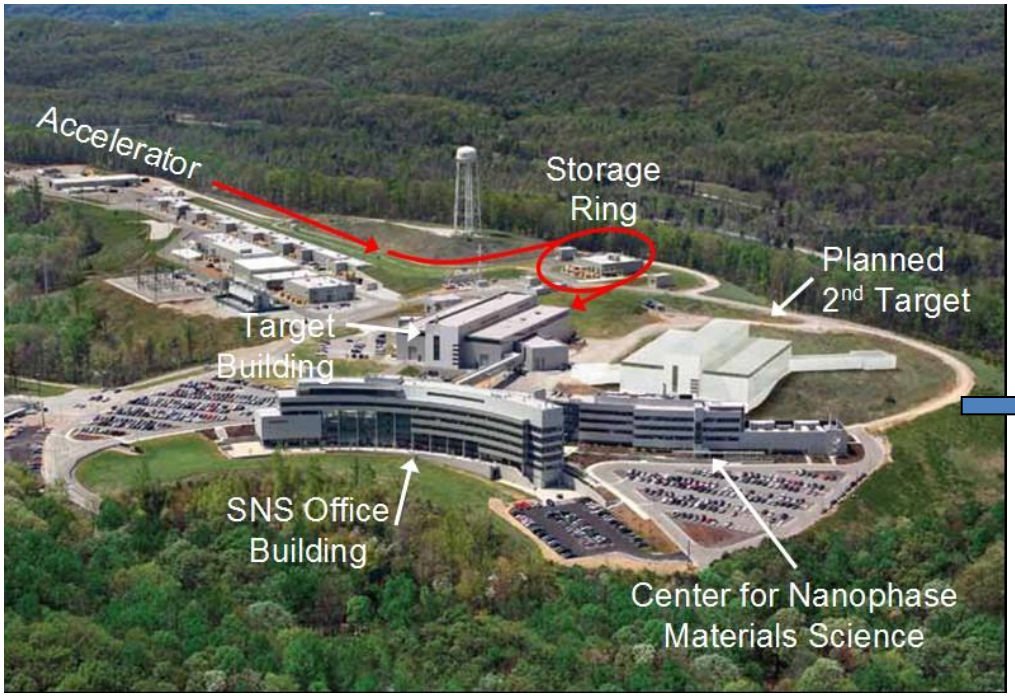

Conceptual design of VULCAN diffractometer

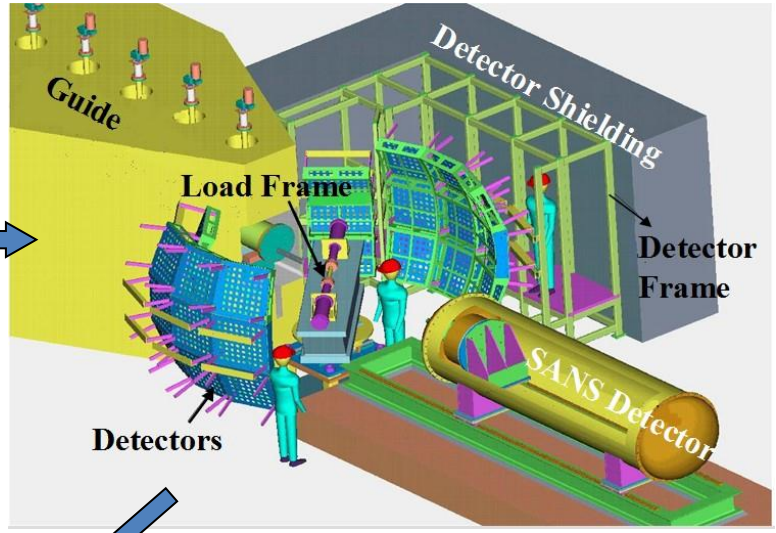

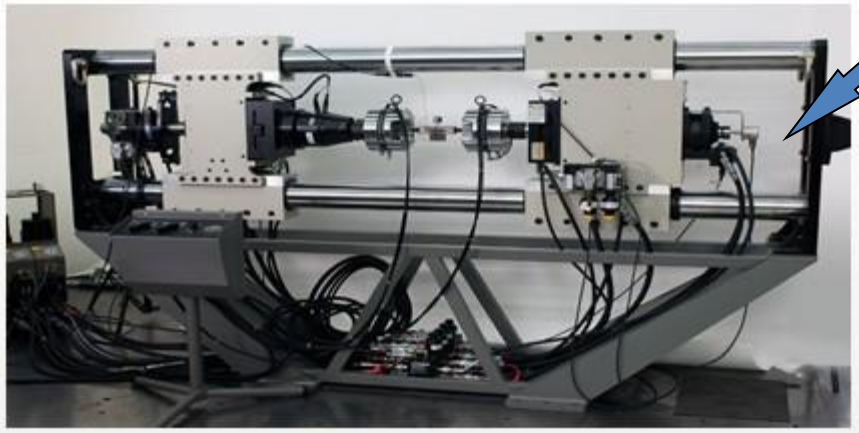

The multifunctional load-frame developed for VULCAN diffractometer

Proposed Neutron-Diffraction Studies (with NU Team)

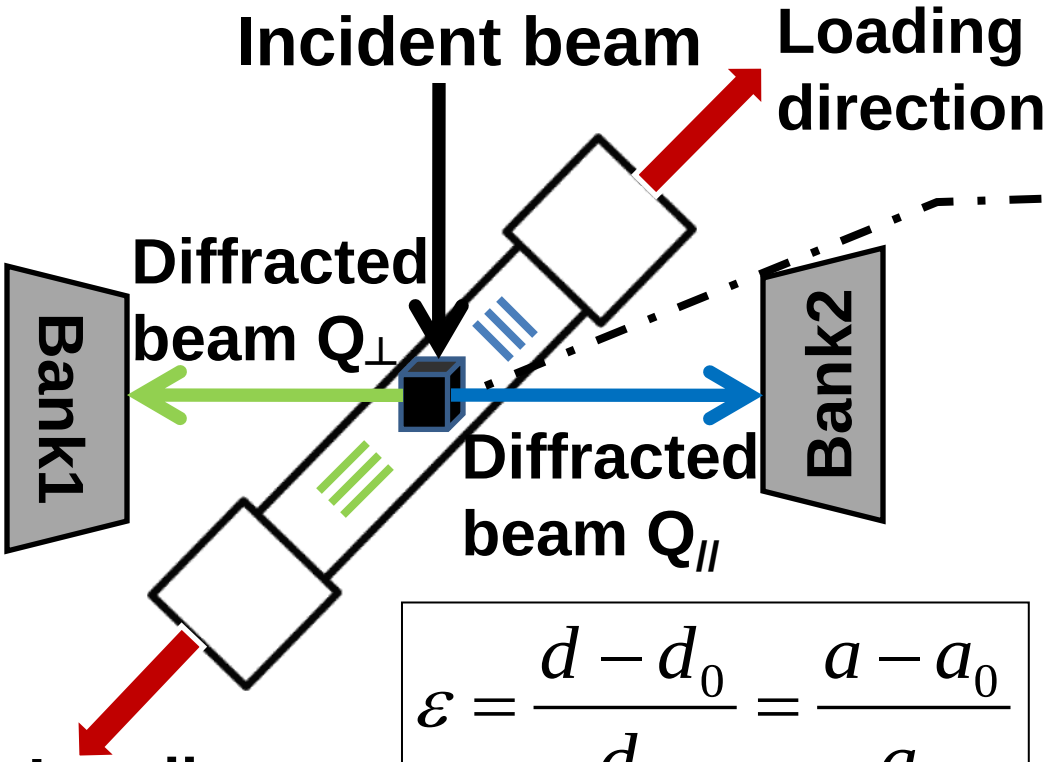

$$\varepsilon = \frac{d - d_0}{d_0} = \frac{a - a_0}{a_0}$$

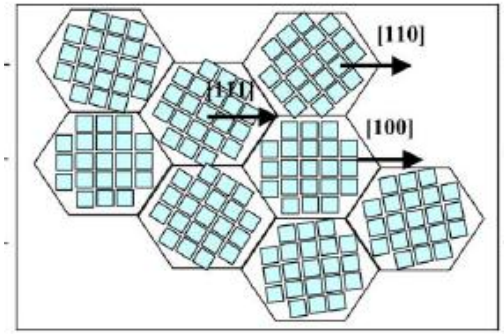

Phase strain

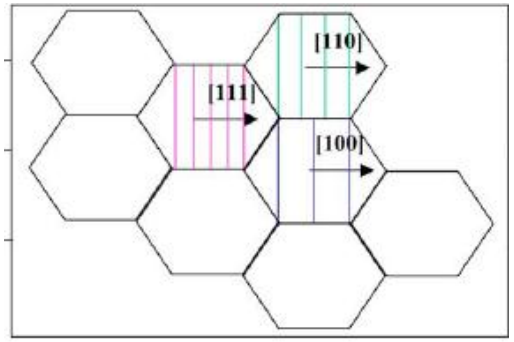

Plane specific strain

Neutron diffraction provides direct measurements of elastic strains (lattice strains). Peak position, width, and intensity are obtained.

Proposed Neutron-Diffraction Studies (with NU Team)

- Information directly and indirectly (coupled with finite element modeling) determined by in-situ neutron diffraction during tension and creep:
  - Lattice strain (phase and hkl plane-specific strain) and stress
  - Lattice misfit between the matrix and precipitates
  - Phase volume fractions
  - Texture evolution during deformation
  - Load partitioning among phases
  - Elastic moduli of constituent phases
  - Critical resolved shear stress

Project Budget and Schedule

Project Funding Profile (Unit: $K)

Years	Total ($K)
2011	357
2012	420
2013	423
Total ($K)	1, 200

Project Management Plan

Project Timeline

Tasks	2011				2012				2013			
Task 1: Thermodynamic Modeling of Multicomponent, Multiphase Alloys												
- Bulk thermodynamic properties												
- Interfacial free energies												
- APB free energies												
- Elastic constants												
Task 2: Kinetic Modeling of Multicomponent Alloys												
- Impurity diffusivities												
- Interdiffusion coefficients												
- Integration of computational thermodynamics and kinetics												
Task 3: Preparation and Processing of Prototype Alloys												
Task 4: Microstructural Characterization												
- HR-AEM, LEAP, and TEM												
- XRD												
- USAXS												
Task 5: Creep Behavior												
- Creep/tensile experiments												
- Neutron-diffraction study												
- Dislocation-dynamics simulations												

Milestone Log

Milestone Designation	Milestone Description	Planned Completion Date
1	Thermodynamic modeling of bulk thermodynamic properties	06/30/13
2	First-principles calculations of interfacial free energies	12/31/12
3	First-principles calculations of APB free energies	06/30/13
4	First-principles calculations of elastic constants	06/30/13
5	First-principles calculations of impurity diffusivities in Fe	03/31/12
6	Kinetic Monte-Carlo simulations of interdiffusion coefficients	06/30/13
7	Integration of computational thermodynamics and kinetics	06/30/13
8	Fabrication of the designed alloys: A. base composition; B. modified compositions	A. 12/31/11 B. 06/30/13
9	Chemistry, partitioning, precipitates, grains, and dislocations characterized by HR-AEM, LEAP, and TEM	12/31/13
10	Lattice-parameter and volume-fraction measurements by XRD: A. base composition; B. modified compositions	A. 12/31/11 B. 09/30/13
11	Quantification of precipitates by USAXS	03/30/13
12	Creep/tensile experiments	06/30/13
13	Neutron-diffraction study of creep behavior	09/30/13
14	Dislocation-dynamics simulations of creep properties	12/31/13

Project Risks and Risk Management Plan

Potential Risks and Management

- Facility/Equipment Failures
  - Monthly equipment testing and maintenance procedures
  - Recording of equipment use history
  - Checking and repairing by trained technicians or manufacturer
  - Arranging alternative equipment
- Beam Time for Neutron/Synchrotron Experiments
  - Submitting proposals to national and international neutron and synchrotron facilities
- Delay of Proposed Computational Tasks
  - Major causes: the maintenance of supercomputing or cluster facilities and jobs waiting for a long time to be executed in the queue
  - Utilizing various computational resources to lower the risk

Conclusions

Conclusions

- The proposed B2 or/and $L2_1$ precipitates strengthened ferritic alloys are promising for the elevated-temperature applications.
- Modern computational tools and algorithms will be developed and integrated to promote the development of novel high-temperature alloys for fossil-energy applications.
- Creep experiments, advanced characterizations , and quantitative modeling will be conducted to achieve a fundamental understanding of the creep behaviors of novel ferritic alloys and validate computational results.

Q & A

Project Tasks (1)

- **Task 1:** Integrated Design
  - Building upon our prior work, and in collaboration with other team members (PIs and students), this task will focus on the integration of computational and experimental results leading to the design and prototype evaluation of ferritic superalloys with the dispersion *B*2 and/or $L2_1$ precipitates.

- **Task 2:** Thermodynamic Modeling of Multicomponent, Multiphase Alloys
  - This is a computation-intensive task. Both first-principles and CALPHAD-type computational thermodynamics and kinetics computations will be carries out. In-house computational resources and national facilities, such as TeraGrid and National Energy Research Scientific Computing Center (NERSC), will be utilized in this task.
  - The approach involves integrating first-principles calculations and experimental data to develop computational thermodynamic databases, which forms the framework for CALPHAD modeling of multicomponent phase diagrams and thermodynamic properties.
  - Prof. Asta will collaborate with Prof. Ghosh on above computational work.

Project Tasks (2)

- **Task 3:** Kinetic Modeling of Multicomponent Alloys
  - This task is to develop first-principles computations to predict the diffusivities and interdiffusion coefficients in bcc-Fe binary alloys.
  - For the purposes of alloy design, this information can be integrated with available experimental data to develop accurate kinetic databases for the DICTRA-based simulations of diffusion-limited processes in multicomponent systems.
  - Prof. Asta will lead this effort.

- **Task 4:** Preparation and Processing of Prototype Alloys
  - Sizable ingots will be fabricated with proper melting and heat treatments.
  - The alloys will be prepared by Sophisticated Alloys, Inc.

Project Tasks (3)

- **Task 5:** Microstructural Characterization
  - Combined TEM/AEM, atom-probe tomography (APT), XRD, and USAXS experiments will be performed in this task. Both in-house and national facilities, such as Argonne National Laboratory (ANL), Oak Ridge National Laboratory (ORNL), and National Center for Electron Microscopy (NCEM), will be utilized for required experiments.
  - State-of-the-art electron-microscopy studies will be undertaken at NCEM to investigate deformation microstructures and the structure and composition profiles at precipitate/matrix interfaces.
  - The results will facilitate a quantitative comparison between computational predictions and experimental measurements, which will assist in developing processing-microstructure-property-performance relationships.

- **Task 6:** Creep Behavior
  - Creep experiments will be conducted.
  - Carry out the neutron-diffraction study to investigate the relationships among the microscopic elastic-lattice strains, microstructure evolution, and macroscopic creep behaviors.
  - Perform dislocation-dynamics simulations to predict the creep behaviors.

Neutron and Synchrotron Facilities (3)

High temperature neutron diffraction experiments at Engine-X, ISIS, Rutherford Appleton Laboratory, UK

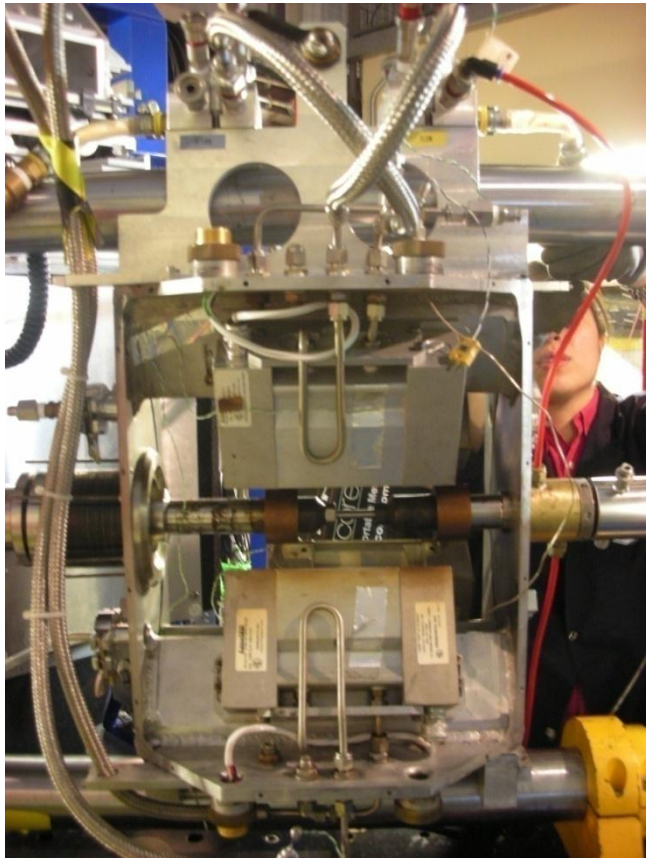

SMARTS, Los Alamos National Laboratory

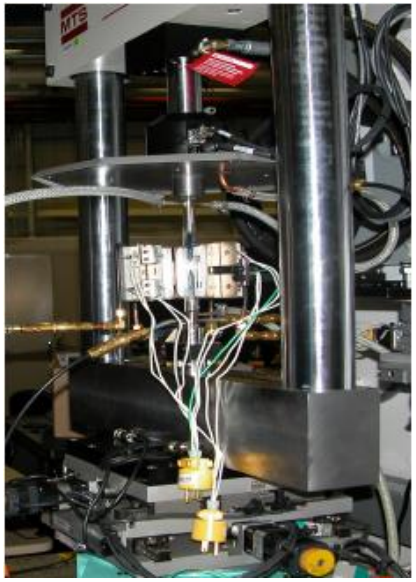

1ID-C, thermo-mechanical device, Advanced Photon Source, Argonne National Laboratory